CYCLIC LOADING OF PORCINE CORONARY ARTERIES

A Thesis
Presented to
The Academic Faculty

By

Crystal M. Gilpin

In Partial Fulfillment
Of the Requirements for the Degree
Master of Science in the
School of Mechanical Engineering

Georgia Institute of Technology

May 2005

CYCLIC LOADING OF PORCINE CORONARY ARTERIES

Approved by:

Dr. David Ku, Chair
School of Mechanical Engineering

Georgia Institute of Technology

Dr. William Steven Johnson
School of Materials Science and Engineering
Georgia Institute of Technology

Dr. Raymond Vito
School of Mechanical Engineering
Georgia Institute of Technology

Date Approved: April 5, 2005

This work is dedicated to Anoopa Denise Sharma.

ACKNOWLEDGMENT

Thank you Mom, Dad and Justin for all of your support, love and encouragement. I would not be here without you.

Dr. Ku, thank you for your guidance, encouragement and words of wisdom. Thank you Dr. Rachev for your patience and your constant willingness to help. Conor and Rahul you made me laugh when I wanted to pull my hair out, I couldn't have asked for better friends. To Dr. Y's lab and Dr. Vito's lab thank you for teaching me along the way. To Dr. Levenston and lab, especially Chris, thank you for all of your help. Dr. Guldberg and lab, thank you for letting me do my testing uninterrupted for months. Angela thank you for your help and Srin, thanks for talking to me while I was cycling. Tracey Couse, thank you for doing everything that you could do to make my research successful. Segried and Glenda you keep things going, thank you for making my time here run smoothly.

To my friends who have become family here in Atlanta, Dr. Watkins, Dr. Hite, Dr. Babalola, Meteorologist Dana Long, Ms. Makayah Royal, Dr. McCoy and Matt Hammond. Thank you for encouraging me and listening to me complain. Robyn, words can not explain what an angel you have been to me- thank you. Hardy family, you made me feel at home. Thank you for taking me in and feeding me when I didn't want to be near campus. Shontya' and Brian my thesis is finished because of you, Shontya'- we did it! Summer I am waiting for you to be typing this page; it's my turn to encourage you- hang in there!

God Bless you all!

"…To whom much is given much is required…" – Luke 12:48

TABLE OF CONTENTS

LIST OF TABLES

LIST OF FIGURES

LIST OF SYMBOLS

A_o	Initial Area
A	Final Area
V_o	Initial Volume
V	Final Volume
λ	Stretch Ratio of Circumferences
C_o	Initial Circumference
C	Final Circumference
w_o	Initial Width
t	Time
S_o	Engineering Stress
S	Final Stress
P	Pressure
r	Radius
H	Initial Thickness
h	Deformed Thickness
TT	Tensile Test
CT	Cyclic Test

SUMMARY

Fatigue is the process of damage accumulation in a material that is subjected to cyclic loading. Cyclic loading occurs in soft tissue and can lead to failure of the material. Failure of soft tissues can cause life threatening events such as the rupture of an aneurysm or plaque cap rupture, leading to a myocardial infarction or Sudden Cardiac Death. The structural components of arteries and plaque caps are collagen and elastin. There has been little work done on the fatigue failure of soft tissues.

Porcine coronary arterial rings, ranging 3-5 mm in diameter, were pulled to failure in tensile tests to determine their ultimate strength. The ultimate load range was 9.91 $\pm$ 5.76 N and the ultimate strength range, based on an average cross-sectional area of 4.1 $\pm$ 1.4 mm^2, was 1.48 $\pm$ 0.49 MPa. The average stretch ratio of circumferences of the rings tested in tension was 2.06 $\pm$ 0.63.

Arterial rings were also cycled to failure at various loads. The Number of Cycles to Failure ranged from 3 cycles at 80% of the ultimate load, to 65,280 cycles at 28% of the ultimate load. Histology of cycled samples showed the accumulation of fatigue damage in the tissue. Weakening of the tissue was also exhibited by a positive slope of successive plastic deformation in the Position vs. Time plot. This positive slope, or creep, predicts that the material will eventually fail. The magnitude of the slope indicates how quickly the material will fail. The correlation between the %Load and the Number of Cycles to Failure may be used to predict when the artery will fail.

CHAPTER 1

INTRODUCTION

Fatigue is the damage and failure of materials that are subjected to cyclic loads. This definition has evolved from one that primarily pertained to metallic materials in 1964 [1], to now include metallic composites [2], polymers and soft tissues.

The process of fatigue failure is different depending on the structural unit of the material. Metals and solids are composed of crystals that slip past one another in irreversible ways forming cracks which initiate and propagate until the material fails. The structural components of polymers are long chains of molecules with modes of irreversible deformation that differ from metals. For example, while metals can undergo cyclic softening or hardening, polymers only undergo cyclic softening. This cyclic softening behavior lasts for the entire fatigue life of a polymer-matrix, so it never reaches a state of equilibrium. Soft biological tissue is often modeled using polymer materials [3]. The primary structural components of soft tissue, elastin and collagen, have elastic and plastic deformation properties that are most similar to polymers. Some soft tissues, such as arteries, have a polymer-matrix, or composite, type structure because they are made of layers of material similar to polymers. As with polymer-matrix materials, soft tissue has been shown to fatigue [4] and to cyclically soften [5].

Fatigue failure accounts for the majority of failures in machinery and structural components [1]. In addition, the stresses at which the components are cycled is often well below the values which are considered to be ‘safe’. This is of particular concern in

the body, because cycling at stresses that are expected to be safe can lead to unexpected rupture of soft tissue.

A condition where tissue expands and eventually ruptures is called an aneurysm. An aneurysm is a bulge or ballooning at a weak area of a vessel wall. The eminent threat of aneurysms is rupture because this event can lead to a massive hemorrhage causing a stroke or death. Aneurysms frequently occur in the thoracic and abdominal portions of the aorta and in the brain. An aneurysm can be caused by atherosclerosis. Atherosclerosis is a disorder where fat is deposited in the vessel wall and the lumen of the vessel is narrowed. These changes in the vessel wall and blood flow can weaken other areas of the wall and cause an aneurysm to form. The rupture of the aneurysm is currently unpredictable, although the formation of the aneurysm can be detected. Another condition where the rupture of tissue is important is plaque cap rupture. Plaque caps form over the fatty deposits in the vessel wall that are characteristic of atherosclerosis, and their rupture is a potentially life threatening event.

Background

Soft Tissue

There are four primary types of tissue in the body: epithelial, connective, muscular and neural. Epithelial tissue provides protective barriers for organs and other tissue structures such as skin. Connective tissue is found throughout the body providing structure, protection, storage and transport. Muscular and neural tissues are much more specialized for the functions their names imply, muscular tissue for contraction and

neural tissue for the conduction of electrical impulses. The current research will be focused on the mechanical properties of structures made of connective tissue.

Connective tissue has a fluid component called ground substance which surrounds the structural components, extracellular protein fibers, of the tissue. The three fibers found in connective tissue are collagenous, reticular and elastic fibers. Tendons and ligaments, which can withstand substantial forces, are comprised almost entirely of collagen fibers. Blood vessels also include a monolayer of cells called the endothelial layer. This layer is generally thin and does not provide mechanical structure.

Soft Tissue Mechanics

With such varied functions in the body it is logical that the mechanical properties of soft tissue are not easily defined nor are they uniform. Experiments performed on soft tissues have indicated that they are not linear, or Hookean, solids. Under uniaxial loading the stress in soft tissues increases faster with increasing strain, thus demonstrating a nonlinear stress-strain curve that does not follow Hooke's Law [6]. It has also been shown that in the initial cycles of a cyclic test on soft tissue, the stress strain curve forms hysteresis loops, which continually decrease and then stabilize. This period, leading to repeatability of the stress-strain curve, is called preconditioning. To reach a point of repeatability and to ensure a similar strain history for all samples, mechanical tests of soft tissues are generally performed on preconditioned samples.

The shape of the stress-strain curve as well as the initial hysteresis shows that soft tissues are not linearly elastic. Soft tissues also experience stress relaxation, which means that the stress in a soft tissue that is rapidly strained and then held at constant strain will decrease. In the same manner, the strain of a soft tissue that is rapidly stressed

and then held at a constant stress will decrease, this phenomenon is called creep. The creep, hysteresis and stress relaxation of soft tissue are the reasons that it is defined as viscoelastic.

A material that has the same properties at all points within the solid is homogeneous and if the properties are the same in every direction then the material is isotropic. Soft tissues are composed of layers of different types of tissue made of different cells and fibers. Therefore, in addition to being non-linear, and viscoelastic, soft tissue is non-homogeneous and anisotropic.

Viscoelasticity is a basic type of deformation. Two other types of deformation are elastic and plastic deformation [50]. In elastic deformation the chemical bonds of a material are not broken and the material returns to its pre-stressed state once the load is removed. In plastic deformation the breaking of the chemical bonds causes irreversible deformation, so the material does not return to its pre-stressed state once the load is removed. Elastic deformation generally occurs at low strain values. High strain values lead to plastic deformation that can result in fracture of the material. The highest stress attained prior to this fracture point is the ultimate strength of the material. The ultimate strength for many soft tissues has been defined and is determined for porcine coronary arteries in this research.

Arteries

Many studies have been performed to determine the mechanical properties of arteries. Being comprised of soft tissue, arteries have all of the same properties as soft tissues; they are non-homogenous, non-linear and anisotropic [7], making the definition of their mechanics challenging. An understanding of the structure of arteries is important

in determining their characteristics. However, both the structure and composition varies depending on the location of the vessel in the body. Therefore, failure behavior, such as fatigue failure, will also be different.

Arterial Structure

Arteries may appear homogeneous at the macroscopic level however they are composed of three distinct layers of tissue. The innermost layer of the artery is the intima, made of a layer of endothelial cells that provides a non-thrombogenic surface so that blood can flow through the artery without forming a thrombus, or clot. The thickness of each layer varies depending on where the vessel is located in the body, but the intima is always the thinnest layer and does not normally contain elements that would allow it to contribute to the mechanical properties of the artery. However, the intima can thicken with age and disease which can affect mechanical properties. The media is the middle layer of the artery, provides a great portion of the mechanical properties. This layer is made of smooth muscle cells, elastin fibers and collagen fibrils. Adventitia, the outermost layer, tethers the vessel to surrounding tissue. In arteries the adventitia is comprised of collagen and elastic fibers, and in veins this layer also includes smooth muscle cells.

Elastin is known as the most linearly elastic biosolid material. Organized as filaments in the body, it provides tissues with elasticity at stretch ratios up to λ=1.6 [8] and [6]. Collagen provides mechanical structure in both hard and soft biological materials. Collagen is organized into fibrils which make up larger fibers and is the main load bearing component in blood vessels. Both arteries and veins are composed of smooth muscle cells, elastin and collagen; the main differences between the two are that

arterial walls are thicker, contain more elastic and contractile ability and generally do not collapse. There are differences amongst arteries as well. Elastic or conducting arteries are large in diameter, up to 2.5 cm, very resilient and are primarily used for transport of large volumes of blood from the heart; whereas muscular arteries distribute blood to organs and muscle, are characterized by more smooth muscle cells and are generally 3-10 mm in diameter.

Arterial Mechanics

There are different types of arteries depending on the location in the body and the role of the artery [6] and [8]. In muscular arteries the adventitia makes up as much as 50% of the wall thickness [9]. Arteries closer to the heart have a larger amount of elastin for pulse waves and peripheral arteries have less [6]. The mechanics also change along the length of the artery and depending on whether the stress is in the longitudinal or circumferential direction [10] and [11].

One of the characteristics that distinguish arterial tissue is that its strain properties are not significantly affected by changes in the strain rate. The lack of effect of strain rate on the extension ratios of aortas was demonstrated by Mohan and Melvin using uniaxial testing methods [12]. Two other properties are that arterial walls adapt to stress and have residual stresses. The adaptation of arterial walls to changes in stress is called remodeling. It is generally accepted that artery walls remodel their geometry, structure and composition to adapt to changing load conditions, and research has shown that this remodeling extends to hypertensive conditions [13]. Residual stresses in the artery are seen when the artery is cut open, this opening angle demonstrates the zero-stress state of the artery [6].

The remodeling of the artery is one of the few properties that are limited to live tissue. The other properties are also seen in dead tissue and therefore affect the passive properties of soft tissue. Passive properties depend on the collagen and elastin content of the tissue, smooth muscle cells contribute little. While the collagen-elastin content of the tissue is key in determining the tissues mechanical properties other factors such as individual differences in components, relative composition, and the arrangement of components also play a role [14]. There are also many outside factors that affect the mechanical properties of individual arteries such as animal species, age and diet. In the current work passive mechanical properties will be determined.

Atherosclerosis

Atherosclerosis leads to major coronary artery events such as myocardial infarction (MI), sudden cardiac death (SCD) and coronary heart disease (CHD). Occlusive thrombi that are associated with ruptured atherosclerotic plaques are the most common cause of acute myocardial infarction, sudden cardiac death and unstable angina. Plaque rupture is defined as the development of a tear in the soft tissue covering the fatty deposit of the plaque. This tear exposes red blood cells to the underlying composition, resulting in the formation of a thrombus. The fact that cracks in the soft tissue over a plaque leads to thrombus formation has been known for many years [15]. However, the significance of the progression of the crack as related to major coronary events has become a primary concern within the last 25 years.

Atherosclerotic Plaque Formation

Endothelial cells line the walls of arteries and provide an interface between the blood flow and the underlying tissue. Endothelial cells are responsible for the secretion,

production and metabolism of various molecules and cytokines, as well as providing a surface that resists the formation of clots and controlling the contraction of vascular smooth muscle cells. Cellular interactions, enhanced by risk factors such as diabetes, smoking, hypertension and hypercholesterolemia, can lead to endothelial dysfunction. This condition may lead to the formation of lesions along the endothelium of the vessel wall, an injury that elicits an inflammatory response. The inflammatory response begins with the adherence of monocytes, which transform to macrophages to get rid of foreign substances, and T-lymphocytes, another key cell in the response cascade. The macrophages and T-cells migrate under the endothelium, into the intimal layer, where the macrophages ingest excess lipids and become foam cells. The migration of the cells into the intima is invoked by the presence of oxidized low density lipoproteins on the damaged endothelial layer. Since the injury is not healed on the surface the inflammatory response remains activated, the cells continue to accumulate subendothelially along with smooth muscle cells and extracellular matrix, and the lesion becomes a plaque formation.

Plaque Composition

The composition of the plaque, also called the lipid pool, is water, phospholipids, cholesterol monohydrate, cholesterol esters, and lipids [16]. Cholesterol monohydrate exists as crystals and can have a stiffening effect on the lipid pool, whereas cholesterol esters are oils. This combination, which can also be integrated with fibrous tissue, presents a soft "gruel" that has the consistency of toothpaste at room temperature, and is softer at body temperature [17]. The composition, like the plaque itself, is heterogeneous and varies from subject to subject, and these differences affect the mechanical properties of the vessel wall [18] and [17]. The plaque protrudes further and further into the lumen

of the artery as it forms, narrowing the passageway for blood. This narrowing of the lumen leads to a condition called stenosis. Although vessels can become severely stenosed, it has been proven that degree of stenosis does not directly correlate to plaque rupture [19] and is therefore not the most threatening part of the disease. The reason that plaque rupture is the most life threatening event is because the contact between the lipid pool and blood cells forms a clot or thrombus. A thrombus in arteries is very dangerous because it can occlude the lumen stopping the flow of blood to the heart and leading to a stroke, myocardial infarction, or sudden cardiac death.

Plaque Cap Composition

The structural components of plaque caps are collagen and elastin. Under conditions such as atherosclerosis these are the elements that are being cycled to failure. The structural components of the artery wall are also collagen and elastin. Therefore, in the current work, arteries are tested as a material that is similar in composition to plaque caps. Arteries are also tested because rupture of the arterial wall can occur, such as with aneurysms, so characterization of the failure behavior of the arterial wall is useful for both atherosclerotic and aneurysm applications.

Plaque Rupture

Plaque rupture is the potentially life threatening event that occurs when a tear forms in the soft tissue covering the fatty deposit of the atherosclerotic plaque. This tear exposes the blood in the artery to the lipid pool and causes thrombus formation. While the relationship between plaque rupture and thrombus formation has been established [20], the question of exactly what causes plaque rupture remains unanswered. Since the material in question is a soft tissue there are many biological factors to consider in the

progression of plaque rupture. One theory of plaque rupture is that vascular channels in the atherosclerotic plaques lead to plaque hemorrhage and subsequent thrombus formation. However, it is not clear if this hemorrhaging is linked to plaque rupture. Work by Lendon et al. [21] has shown that the density of macrophages, an inflammatory cell that degrades foreign objects, in the plaque is related to the chances of plaque rupture. Lee et al. studied the expression of matrix metalloproteinases (MMP's), a cytokine that initiates matrix degradation, in areas of increased stress on plaques. The idea is that increased expression leads to weakened tissue, which in combination with the increased stress causes plaque failure. Biological factors such as macrophages and MMP's change the strength of the tissue therefore affecting its response to mechanical loading. Since there is dynamic mechanical loading of the arterial wall, it is clear that plaque rupture is also affected by mechanical stresses.

It has been proven with angiographic studies that the degree of stenosis in arteries related to a major coronary event is not a reliable predictor of plaque rupture [19]. Angiography was the visualization method used by Ambrose et al., and though it was able to identify stenosed arteries, it is not a good tool in determining a patient's predisposition to plaque rupture since there are factors involved other than the degree of stenosis. One of the other factors that has been proposed as a cause of plaque rupture is the hemodynamic shear force that increases with the narrowing of the artery lumen [22]. While it is clear that shear forces are important, it is likely a step in the progression to, rather than the cause of plaque rupture. The effect of turbulent pressure fluctuations that occur in the artery due to the stenosed region has also been suggested to play a role in developing stresses that rupture the plaque cap [23]. However, these experiments by

Loree et al. were performed under steady non-pulsatile flow conditions, so the pressure effects and behavior under the pulsatile and unsteady flow of the artery is unknown. The hemodynamic shear stress and turbulent flow pressure are external forces acting on the plaque, however there are also forces within the tissue that affect its behavior.

Using computer modeling Richardson, Davies and Born [24] were able to show that the distribution of circumferential tensile stress in the vessel wall changes with the presence of atherosclerotic plaques. In particular, they considered eccentric plaques during systole and found that stress is carried disproportionately causing high tensile stress concentrations at certain points along the circumference of the wall. Lee et al. [25] suggested that variations in mechanical properties of soft tissue are dependent on its composition. Specifically they looked at the effect of tissue stiffness on the mechanical behavior; discovering that frequency-dependent stiffness changes lead to shifts of stress distribution in the plaque. Vito et al. [26] developed a finite element model to determine the effects of geometry and mechanical properties on the stresses of a plaque, and showed that the distribution of shear stress between the inner and outer plaque media is also affected by the stiffness of the plaque. These changes in stress distribution and mechanical properties can lead to very high tensile stresses that are strong enough to rupture plaque caps (>300 kPa, [16]). However, rupture does not always occur at the points of maximum circumferential stress [16].

Fracture in areas that do not correspond to the point of maximum stress can occur due to fatigue [16, 25, 27]. Fatigue failure occurs when a material is cyclically loaded, often at a constant or variable stress magnitude lower than the ultimate strength of the material, and damage to the material accumulates leading to crack propagation and

failure. The aforementioned research has realized that there are a variety of mechanical and biological factors influencing the mechanical properties of soft tissue and that there is a relationship between these dynamic properties and rupture. However, the question of the mechanism leading to rupture remains unanswered. Due to the pulsatile nature of blood flow in the arteries, thus creating cyclic loading of the vessel wall, it has been suggested that plaque caps fatigue in a process similar to that of a metal material [24, 28]. Based on this hypothesis, plaques rupture at the point of fatigue failure and therefore understanding the fatigue behavior could lead to methods of preventing plaque rupture.

In general, the tearing of soft tissues in the body may be due to increased stress and mechanical weakening. The mechanical weakening of the artery may be in part due to biological factors, such as macrophages that degrade the tissue [21] and also due to mechanical fatigue. The stress on the soft tissue over the plaque may be increased because of changes in the distribution of stress that occur as the plaque develops [18]. These stresses weaken the tissue through a process of fatigue as the vessel undergoes contraction and dilation with cyclic diastole and systole. The weakening of the tissue through the process of fatigue could, eventually lead to fatigue failure of the tissue. In atherosclerosis, this failure may be synonymous with plaque rupture.

Overview of the Failure Behavior of Soft Tissues

Understanding the failure behavior of tissue is important in describing the fatigue failure. Several researchers have studied the mechanical properties of arteries using uniaxial, biaxial or pressure inflation techniques [7, 10-12, 29-32]. Mohan and Melvin

[12] performed uniaxial tests on dog bone strips of aortic tissue and determined that the ultimate extension ratios are not affected by strain rate. In further work by the same group [33] using biaxial tests they determined that under uniform biaxial stretch the tissue failed in the circumferential direction. In this research Mohan and Melvin determined the average ultimate stress to be 1.14 $\pm$ 0.32 MPa. Inflation tests by Cox [14] were performed on cylindrical canine artery specimen to determine the dependence of properties on the collagen and elastin composition. He found that while the ratio of collagen to elastin is important for the mechanical properties of the arterial wall, the connective tissue composition is also important.

Quapp and Weiss [34] performed uniaxial tensile tests on human medial collateral ligaments (MCL). Ligaments are primarily made of collagen fibers and they found that when pulled along the fiber direction (longitudinal) the ligaments exhibited typical nonlinear behavior. They also found that the ultimate strength, strain and tangent modulus were much higher in the longitudinal direction than in the transverse direction. Weiss et al. [35] studied the behavior of ligaments under shear loading at different shear rates. In both studies strips of ligament were punched out of the MCL for testing. The tensile and viscoelastic properties of human patellar tendon has been studied by Johnson et al. [36]. They found differences in the mechanical properties of the tendon based on age. The values for the ultimate strength were 64.7 $\pm$ 15.0 MPa and 53.6 $\pm$ 10 MPa for the younger and older group respectively. The strain at failure also varied with age, 14 $\pm$ 6% for the younger group and 15 $\pm$ 5% for the older group.

Itoi et al. [37] performed tests on strips of human supraspinatus tendon. The values of ultimate strength that they determined were much lower than those found by

Johnson et al., ranging from 4.1 $\pm$ 1.3 MPa to 16.5 $\pm$ 7.1 MPa. This result shows the variation of tissue properties depending on the location in the body.

Haut et al. [38] performed tensile tests on ring specimen from the canine aorta. The purpose of these experiments was to determine the effects of hypercholestoremia on the mechanical properties of the aorta. The control experiments offered data regarding the ultimate tensile strength of aorta, 1891 $\pm$ 265 kPa.

Work continues to be done to create models to represent the nonlinear anisotropic elastic behavior of arteries [39].

Fatigue of Soft Tissue

Broom [40] tested dog bone shape specimen from bovine and porcine heart valves (n=6) in tension and accelerated fatigue with a load controlled test. The effects of cyclic loading reduced tissue compliance and to changed the structure of the collagen fibers. To create the accelerated fatigue test the rate of cycling was increased to 35 Hz. more than 25 times the physiologic rate of about 1.2 Hz. More recently, Wells and Sacks [41] have investigated the effects of the fixation pressure of porcine bioprosthetic valves on long-term cycling, using a displacement controlled test. The accelerated cycling in this work was performed at 15 Hz. and the valves (n=10) were cycled up to 200 x 10^6 times. This study concludes that although chemically fixed, it is still possible for collagen fibers to undergo conformational changes under long-term cycling.

The effects of cyclic pressure on the sclera of the eye has been studied by Ku and Greene [5]. Rabbit sclera were subjected to cyclic pressures and exhibited creep and structural weakening. The changes that occur in the eye due to cyclic pressures can lead to the condition of myopia. The findings in the research by Ku and Greene indicate that

there is a point in time where the soft tissue begins to deform plastically. The plastic deformation is time-dependent and occurs at a creep rate that Ku and Greene defined in terms of the stress applied to the material and the activation energy.

McCord [4] researched the effects of cyclic bending on human arteries containing plaque (n=28). The cyclic bending reduced the stiffness of the specimen and changed the mode of failure from a smooth to a ragged tear. Fatigue damage was also noted in microscopic observations. Yokobori et al. [42] cyclically pressurized canine thoracic arteries (n=22) 20,000 times up to 400 mmHg. After cyclic tests they tested dog bone shaped samples for ultimate strength. Yokobori et al. found that the ultimate strength of the artery decreased after being subjected to pulsatile flow of varying amplitude.

Although there has been research performed in the area of fatigue of soft tissues, very few researchers have tested the materials to failure. Testing to failure at various stresses is a method that would provide valuable information for predicting when a soft tissue is likely to fail.

Fatigue Behavior Characterization

There are two main approaches to characterizing fatigue life- the Total Life Approach and the Defect Tolerant Approach. The Defect Tolerant Approach tests materials that have a pre-existing flaw in order to determine how defects grow in the material, only considering propagation of a crack. The Total Life approach considers all of the stages of fatigue, i) initiation ii) propagation and iii) failure, where failure is defined in terms of stress life or strain life.

The strain life test is based on constant strain cycling and is generally used for materials that have a structural constraint. The strain life tests can also be used to

determine the effects of multiaxial cyclic loading. The stress life test is generally used for materials that follow a single load path, and the cyclic loading occurs at a constant stress ratio, R.

$$R = \frac{\sigma_{\max}}{\sigma_{\min}} \qquad (1)$$

R is an indication of the mean stress, σ_m:

$$\sigma_m = \frac{\sigma_{\max} + \sigma_{\min}}{2} \qquad (2)$$

Experimental stress life tests will result in a Stress vs. Number of Cycles to Failure curve (S-N curve). This curve shows the trend of the Number of Cycles to Failure (N) required when a material is cyclically loaded at different stress levels (S). This curve has a negative slope and eventually reaches a stress limit, the endurance limit, below which the material could be cycled infinitely many times (>10^7) [1] without failing. The mean stress can affect the fatigue behavior of a material, shifting the S-N curve. This shift can be quantified using models such as the Gerber, Goodman or Soderberg models [1]. The experimental tests to determine S-N curves can be uniaxial, and the trend of the S-N curve, increasing number of cycles with decreasing stress amplitude, has been shown in non-metallic materials [1]. The stress-life tests used in this research do not consider the mean stress effects.

Hypothesis

Atherosclerotic plaque caps are composed of a composite soft tissue material that becomes subjected to cyclic loading under stenotic flow conditions. Cyclic loading causes the plaque cap to fatigue and eventually fail. The hypothesis of this work is that arteries and plaque caps may fatigue and the fatigue behavior may be predicted by a Stress vs. Number of Cycles to Failure (S-N) curve.

Specific Aims

The goal of this research is to determine the fatigue failure behavior of porcine coronary arteries. Specifically, the aims are to:

1. Determine the Ultimate Tensile Strength of porcine coronary arteries.
2. Subject porcine coronary artery samples to cyclic loading.
3. Determine fatigue behavior by defining an S-N curve for porcine coronary arteries.
4. Compare the morphology of the fatigued and tensile test samples to a control artery sample.

CHAPTER 2

METHODOLOGY

In this work two primary experiments were performed, Ultimate Strength Tests and Cyclic Fatigue tests. Ring specimens were used for all tests because they are easy to obtain from the tubular structure of the artery without the significant damage that could occur from preparing uniaxial dogbone shaped strips. Dogbone strips would also be difficult to obtain because of the small diameter of the artery.

The initial stress in the ring was calculated Failure of the ring specimen was defined as a complete tear of the arterial wall, breaking the ring structure. The final stress at failure represented the ultimate strength for the tension tests and the cyclic stress magnitude for the cyclic fatigue tests. To determine the final stress for the cyclic tests an equation was derived based on the assumption of incompressibility [39]. This assumption means that the initial volume, V_o, and final volume, V, are equal. Using this equality the relationship between the initial and final area can be derived. The derivation is shown in the equations below:

$$V_o = A_o * l_o \tag{3}$$

$$V = A * l \tag{4}$$

Incompressibility: $V = V_o$ (5)

$$A_o * l_o = A * l \tag{6}$$

$$A = A_o * \frac{l_o}{l} = A_o * \frac{1}{\lambda} \tag{7}$$

In the present experiments the lambda, or stretch ratio, is the ratio of the final and initial circumference, Equation (8), since ring specimen were tested.

The final stress, defined by the load at the breaking point of the sample, F_{ult}, as the stress at failure, was calculated using Equation (10) for both ultimate strength and cyclic tests. Generally the final stress is a function of the final load and the final cross-sectional area. However, testing to failure destroys the sample and the final cross-sectional area was not measurable. Therefore, the final stress calculation is a function of the load at the breaking point of the sample, F_{ult}, the stretch ratio and the initial area. The stretch ratio relates the final and initial area due to the assumption of incompressibility. The initial cross-sectional area is the product of the initial width of the sample, w_o, and the initial thickness, H.

$$\text{Stretch Ratio} = \lambda = C / C_o \qquad (8)$$

$$\text{Initial Cross-Section Area} = A_o = w_o * H \qquad (9)$$

$$\text{Final Stress} = S = \frac{F_{ult} * \lambda}{A_o} \qquad (10)$$

The final load normalized to the initial area or the engineering stress, S_o was also calculated using the equations below.

$$\text{Engineering Stress} = S_o = \frac{F_{ult}}{A_o} \qquad (11)$$

In order to get an estimation of the burst pressure in an intact artery the following simplified assumptions were used. It was assumed that a tubular specimen will burst when the circumferential wall stress is equal to the ultimate stress, S. However, when an artery is under physiologic load conditions it is in a state of plane strain and undergoes finite circumferential and axial stretch (Illustration in APPENDIX A). The stretch ratios are:

$$\lambda_\theta = \frac{r}{R} \qquad (12)$$

$$\lambda_z = \frac{l}{L} \qquad (13)$$

The equation for overall equilibrium in the radial directions, which yields the wall stress in the circumferential direction of a tubular specimen is often called the LaPlace equation:

$$\sigma = \frac{\mathrm{Pr}}{h} \qquad (14)$$

where r and h are the deformed radius and thickness respectively. Due to incompressibility:

$$h = \frac{H}{\lambda_\theta \lambda_z} \qquad (15)$$

Substituting Equation (15) into Equation (14) gives the equation:

$$\sigma_\theta = \frac{\lambda_\theta^2 \lambda_z PR}{H} \qquad (16)$$

Rewritten to solve for the pressure, P:

$$P = \frac{H\sigma_\theta}{\lambda_\theta^2 \lambda_z R} \qquad (17)$$

This equation calculates the pressure if the initial dimensions, the ultimate stress and the stretch ratios are given. The axial stretch ratio *in situ,* λ_z , is on the order of 1.5 for the porcine common carotid artery [47]. The circumferential stretch ratio, λ_θ, results from the axial extension to *in situ* length that causes a shrinkage of the artery, and from inflation due to internal pressure. To evaluate the value of λ_θ the experimental results given in Chin Quee's work [47] were used. Chin Quee determined that the circumferential stretch ratio caused solely by extension of the artery to its *in situ* length is on the order of 0.7 ± 0.1. He also recorded that the ratio between the midwall diameter of the artery at the state of bursting and the diameter at zero pressure is on the order of 1.15, when the artery is kept at *in situ* length. Accounting for the fact that the total circumferential stretch ratio resulting from two successive deformations is a product of the stretch ratios corresponding to the individual deformations, it was accepted that $\lambda_\theta = 0.7*1.15 = 0.805$. The values $\lambda_z = 1.5$ and $\lambda_\theta = 0.805$ were substituted into Equation (17) when estimating the corresponding burst pressures.

Ultimate Strength Test

Ring specimens for these tests were pulled in tension until they failed. The load at failure was recorded as the ultimate load, and the ultimate stress or strength of the material was calculated. The purpose of these experiments was to determine a range of stresses for the failure of porcine arteries.

Cyclic Fatigue Test

Ring specimens were cycled to failure at different loads. The frequency of the cyclic tests was set at 1.5 Hz because this value is close to physiologic frequency of heart beats (~1.2 Hz.). The final stress was used as the stress, S, on the Stress vs. Number of Cycles to Failure (S-N) curve. The N was determined from the length of time elapsed before the specimen broke. The purpose of the fatigue tests was to experimentally determine the points defining an S-N curve for porcine arteries. The stress ratio, R for the cyclic tests was 0.

Histology

The histology of control, ultimate strength and cyclic fatigue tested samples were studied. The samples were embedded in paraffin so that they could be sectioned and placed on microscopic slides. A Verhoeff elastic stain and a Van Gieson stain were performed so that the collagen and elastin components of the tissue could be identified. The purpose of these observations was to identify the changes in the tissue components and layers as the fatigue damage from cyclic testing accumulated in the artery.

Experimental Protocol

Porcine hearts were harvested from pigs at Hollifield Farms (Covington, GA). The hearts were transported to the laboratory in coolers packed with ice. The right coronary arteries were excised from these hearts approximately 1-2 hours after harvest. For the excision the right atrium was removed first, followed by the cutting away of surrounding muscle, fat and connective tissue to expose about 80 mm length of artery.

The excision of the artery from the heart was started about 10-15 mm from the junction of the artery and the aorta. The final specimen was about 60 mm in length, due to shrinkage of the artery once it was released from *in vivo* stretch. Excess connective tissue on the artery was removed with a scalpel or tissue scissors. The artery was then stored in Phosphate Buffered Solution (PBS, pH=7.4±0.1) in a refrigerator (5° C) until testing. The PBS (Fisher Scientific) was received as a 10x solution and was diluted to 1 X solution using deionized water to reduce the amount of impurities.

In preparation for fatigue testing the artery was cut into rings 3-4 or 5-6 mm in width using a razor blade. To cut the artery the ends were clamped to hold the artery still, and it was aligned next to a metric ruler. The cuts were made with the razor at the points along the ruler so that the ring was cut to the correct width. After the ring was separated from the artery an additional cutting of excess connective tissue was performed. The rings were stored in proximal to distal order in a segmented culture tray filled with PBS (Figure 1). Testing of the arteries began within 72 hours of harvest.

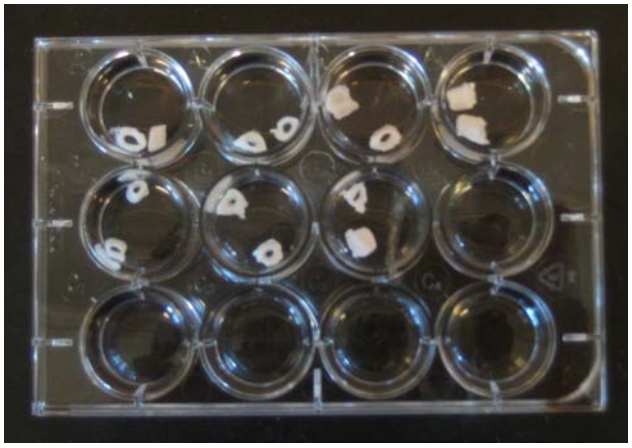

Figure 1: Paired Ring Samples in PBS

The outer diameter (OD), inner diameter (ID) and Width (w) were measured manually for each specimen with digital calipers. A disadvantage to this method of measurement is the possibility that forces applied to the specimen with the calipers caused errors in the measured values. In order to reduce the amount of error, the measurements were taken in triplicate and averaged for use in calculations.

Mechanical Testing

All of the specimen were tested on a servo-controlled electro-mechanical testing machine (Model 100 R, Test Resources, Shakopee, MN). The Model 100 R is a universal mechanical testing machine that can be used to test in tension and compression. The maximum load capacity is 667 N. The load cell used with the testing machine was a 100 N load cell. Although the proportional, integral and differential settings of the machine were calibrated prior to testing there was some error noted during testing between the input and output. This error decreased as the cycling tests progressed. To run the test a load controlled profile was created in the testing software (MTestWR). For the uniaxial test a load profile was setup (Table 1) which preconditioned the specimen 10 times to 0.4 N (Steps 1. and 2. in Table 1) and then loaded the specimen at a rate of 0.4 N/sec until the specimen failed or reached the maximum load of 15 N. The load, position and time information was collected by the computer software at a rate of 5 data points/sec.

Table 1: Ultimate Strength Test Profile

Command	Control Rate (N/sec)	Amplitude (N)	Frequency	Number of Cycles
1. Load	0.4 N/sec	--	N/A	N/A
2. Amplitude	0.4 N	0.4 N	1 Hz	10
3. Load	0.4 N/sec	--	N/A	N/A

Once the profile was set, one specimen from the pair was positioned onto two hooks. The hooks were securely placed into the grips of the machine in a position that placed no load on the specimen (Figure 2). The test was started, ran until failure and the final load was recorded as the ultimate load of the material. This test was performed at room temperature (24ºC) and lasted between 10 and 30 s.

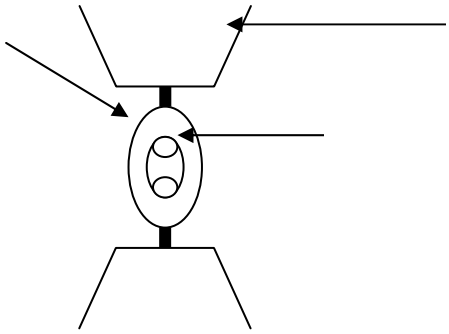

Figure 2: Test Setup
(Diameter of the hook, d_{hook}: 2.62 mm)

For the cyclic test, a profile was created (Table 2) that preconditioned the specimen ten times and then cycled the specimen at an amplitude, L_a, based on a percentage of the ultimate load, F_{ult}:

$$L_a = \%\frac{F_{ult}}{2} \qquad (18)$$

The profile was programmed to ten cycles of preconditioning at 0.4 N (Steps 1. and 2. of Table 2) and then 5000 cycles at the predetermined amplitude, both set of cycles were at a rate of 1.5 Hz. The profile was run repeatedly until the specimen failed. If the

specimen failed before the initial 5000 cycles were run then the test was stopped at that point. All load, position and time data was recorded by the computer. The cyclic tests were performed with the specimen immersed in a bath of PBS to prevent the tissue from drying. Drying out of the tissue would change the mechanical properties. The cyclic tests were also performed at room temperature (24°C).

Table 2: Cyclic Test Profile

Command	Control Rate (N/sec)	Amplitude (N)	Frequency	Number of Cycles
1. Load	0.4 N/sec	--	--	--
2. Amplitude	--	0.4 N	1 Hz	10
3. Load	0.4 N/sec	--	--	--
4. Amplitude	--	L_a	1.5 Hz	5000

The failed specimen from both tests were either prepared for paraffin embedding or discarded. The broken specimen to be embedded, were fixed in 10% neutral buffered formalin for 48 hours at room temperature (24°C). After being fixed they were placed in a tissue processor for dehydration and paraffin infiltration. The paraffin treatment and tissue staining was performed in the Histology lab (Tracy Couse, Histology Lab Director, Georgia Tech, Atlanta, GA).

Data Analysis

All of the collected data was imported into Excel and plots of the Load and Position vs. Time were created. For the tensile tests the plots were used to determine the maximum load and position at failure. For the cyclic tests the total amount of time, t, to

failure (excluding the time for preconditioning) was recorded and divided by the frequency, 1.5 Hz. to determine the Number of Cycles to Failure, N.

$$N = \frac{t}{1.5Hz.} \qquad (19)$$

The final position, L of the cyclic test, shown in Figure 3, was used to calculate the final circumference of the specimen, C.

$$C = (2 * L) + (2 * \pi * (½)d_{hook}) \qquad (20)$$

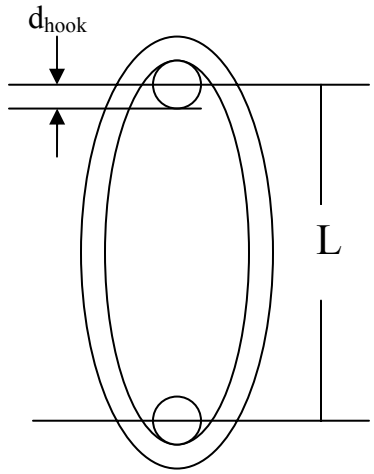

Figure 3: Sample Extended in a Uniaxial Test

The initial circumference, C_o, was calculated as:

$$Co = \pi * \frac{(OD + ID)}{2} \qquad (21)$$

The stretch ratios and final stresses were calculated using the equations above. From the collected and calculated data plots were made to determine the relationship between the stress, the % Load and the Number of Cycles to Failure.

CHAPTER 3

RESULTS

A total of fifteen right coronary arteries were excised from porcine hearts for testing. Eight of the arteries were cut into ring samples about 5 mm in width. The remaining seven arteries were cut into ring samples 3 mm in width. A total of 57 rings were tested.

Figure 4: Right Coronary Artery

Figure 5: Segmented Right Coronary Artery

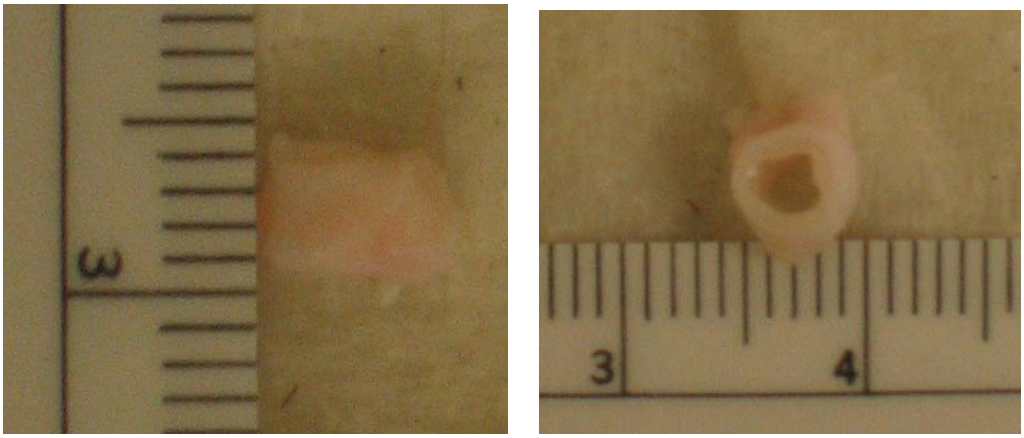

Figure 6: Side and Cross-Sectional View of RCA Segment

Table 3: Average Sample Dimensions

Measurement	Average ± Standard Deviation (mm)
Length	5.1 ± 0.7
Inner Diameter	3.1 ± 0.4
Outer Diameter	4.93 ± 0.5

Mechanical Tests

The rings were cut in proximal to distal order along the length of the artery and adjacent rings were paired. The rings were stored as pairs in a segmented tray filled with Phosphate Buffered Solution (PBS).

From each pair one sample was tested in tension to failure to determine the ultimate strength of the artery; the other sample of the pair was tested in a cyclic fatigue test to determine the Number of Cycles to Failure. The number of ring samples cut from each of the arteries and the type of test performed on each is outlined below in the Artery Tables (APPENDIX B). The samples are labeled in proximal to distal order, 1 being most proximal to the root of the artery.

Ultimate Strength Tests

Thirty-six rings were tested for ultimate strength. The test was stopped when the sample failed. Failure of the sample was defined as a tear through the thickness of the artery wall so that no tissue was connected across the tear, completely breaking the ring structure (Figure 7). This separation occurred most frequently along the straightened walls of the artery, not at the hooks.

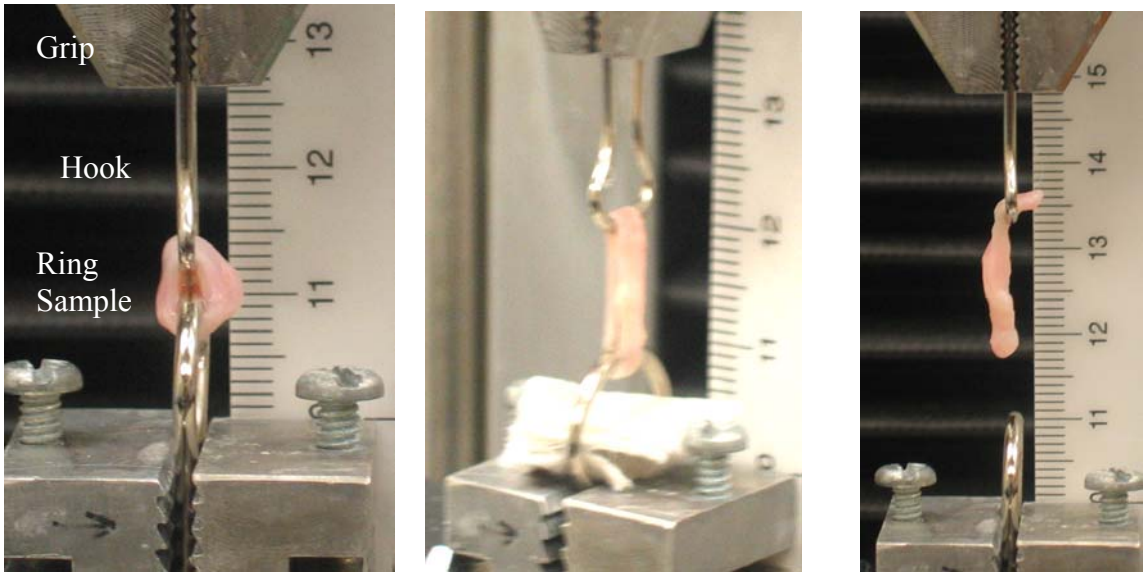

a. **b.** **c.**

Figure 7: Progression of Artery Failure

a.) Artery placed on the hooks. The hooks are secured in the grips of the machine. b.) Artery being pulled during a tensile test. An absorbent towel is placed under the sample to absorb excess PBS c) Failure of the artery

The load and change in position of the grip were measured directly by the computer for every sample. An example of these plots for the Ultimate Tensile Strength (UTS) Test on Artery L is shown in Figure 8 and Figure 9.

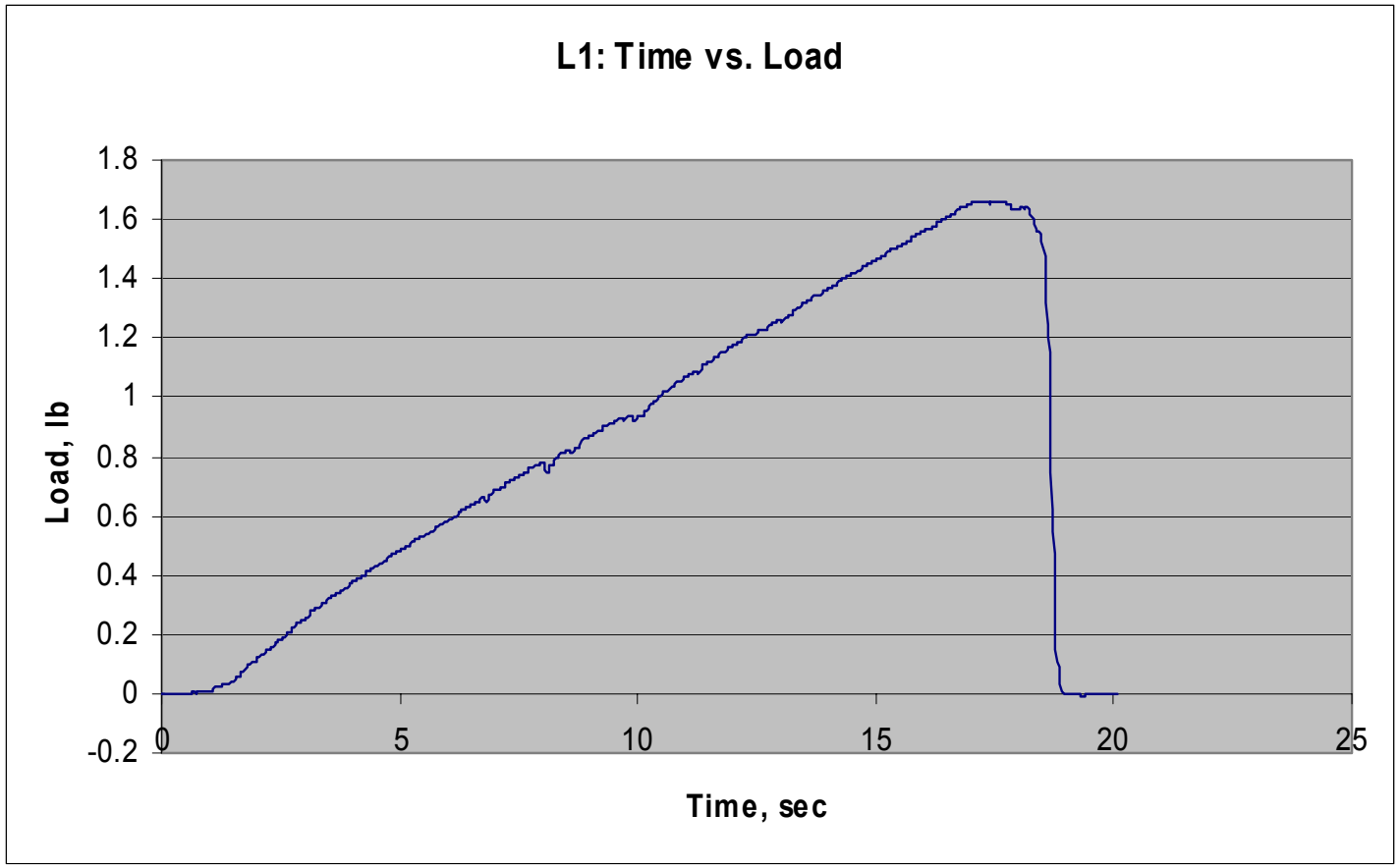

Figure 8: Artery L1 UTS Test

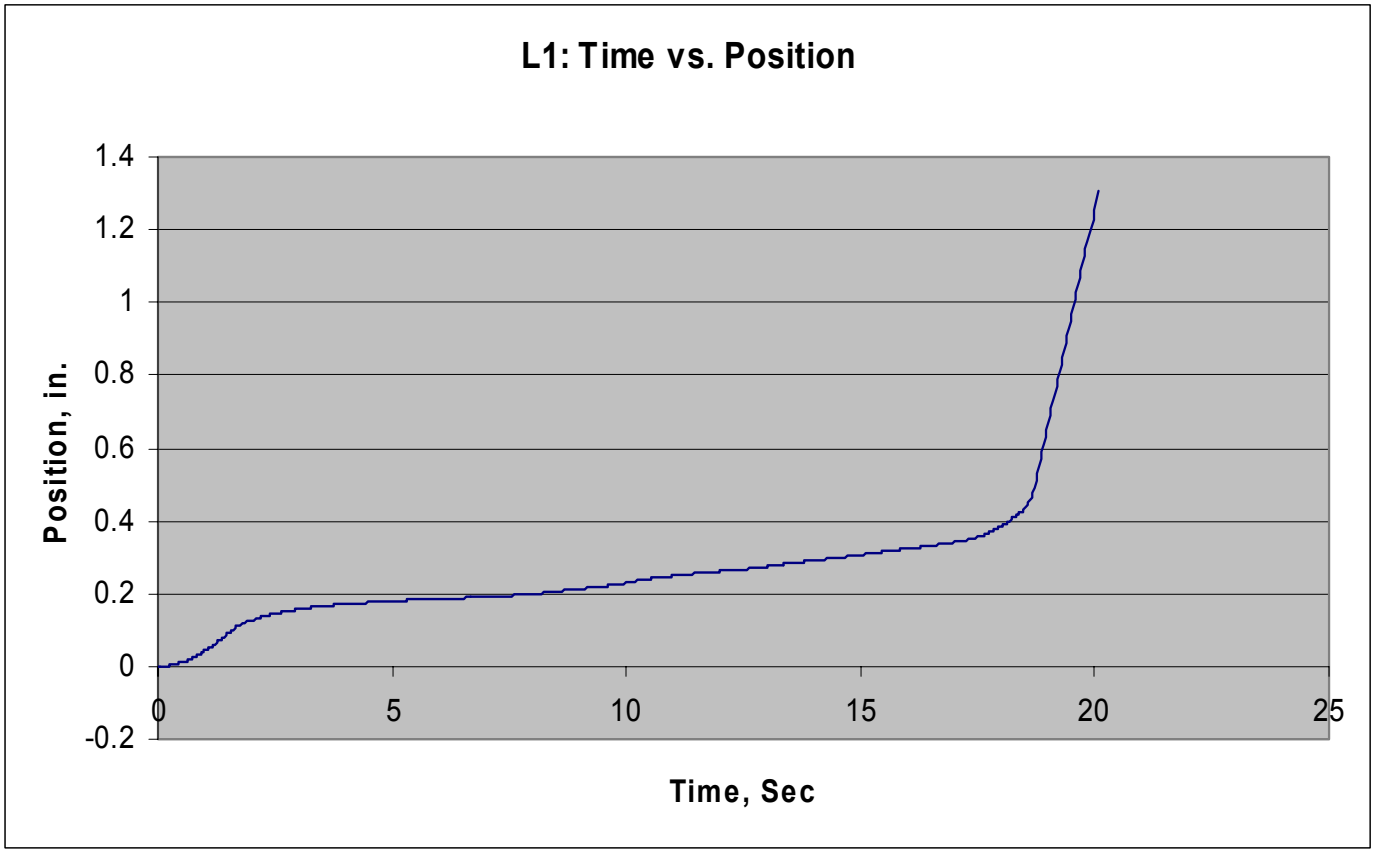

Figure 9: Artery L1 UTS Test

The stretch ratio for each artery was defined as the ratio of the final and initial circumference. The initial circumference was calculated from the measured outer diameter, inner diameter and length. The final circumference was calculated from the length of the artery walls at failure and the diameter of the hooks holding the sample (see Figure 3). The average stretch ratio was 2.06 $\pm$ 0.6.

The maximum load applied to the sample before it failed was recorded as the ultimate load. The stress at failure was calculated from the ultimate load using the stretch ratio and the initial cross-sectional area. This stress defined the ultimate strength of the artery. The ultimate loads at failure ranged from 2.31 N (0.52 lb.) to 25.27 N (5.68 lb.). The average ultimate load was 9.91$\pm$ 5.7 N (2.23 $\pm$ 1.2 lb.). The calculated ultimate strength of the samples ranged from 0.46 to 2.55 MPa, with an average of 1.17 $\pm$ 0.5 MPa.

The pressure in the sample was calculated based on the final stress. The average pressure values based on the ultimate strength tests were 3814 $\pm$ 2214 mmHg (0.5 $\pm$ 0.3 MPa).

A table of all measured and calculated data used to determine the ultimate strength and pressure for artery L1 is listed in Table 4 as an example. Testing data for all other arteries is listed in the APPENDIX C.

Table 4: Data for Artery L1

Date of Testing	12/15/2004
Specimen	**L1**
Test	1.00
ID (mm)	3.44
OD (mm)	5.46
Width, b (mm)	5.10
Thickness, t	2.03
Initial Circumference, c	13.98
Final Position (in)	0.35
Final Position (mm)	8.86
Final Circumference (mm)	25.96
Final Force (lb.)	1.66
Final Force (N)	7.40
Stretch Ratio	1.86
Stress (MPa)	0.66
Initial Stress, MPa	0.72
Pressure, MPa	0.30
Pressure, mmHg	2271

Cyclic Fatigue Tests

Fourteen ring samples were cyclically fatigued. The cyclic fatigue test cycled the sample to failure at a constant load. The Load, Position and Time data from these tests were collected by the computer. The plots of this data for artery L is shown in Figure 10 and Figure 11. The Time vs. Position plot has a positive slope as the sample length increased to maintain a constant load acting on the sample. The constant load for the cyclic test was determined as a percentage of the ultimate load of the adjacent sample. The percentage of the ultimate load used for the constant load ranged from 20%-90%. The samples were cycled at a frequency of 1.5 Hz. The Number of Cycles to Failure ranged from 3 to 65,000, depending on the magnitude of the constant load and the stress

experienced by the artery. The percent used to determine the constant load is listed in the Artery Tables (APPENDIX B) for each sample that was cyclically loaded.

The Number of Cycles to Failure, N, vs. Load and % Load are plotted in Figure 12 and Figure 14. The Log(N) vs. Load and % Load are plotted in Figure 13 and Figure 15. Each of these graphs have a negative slope and the linear relationship between the variables is denoted by r. The r value of the Log(N) vs. Initial Stress is 0.534, for the Log(N) vs. % Stress r = 0.484, for the Log(N) vs. Stress r=0.471, and for the Log(N) vs. % load r=0.856.

The initial stress in the material was calculated from the constant load and the initial cross-sectional area of the sample. The average initial stress was 0.7 ± 0.5 MPa. The initial stress values ranged from 0.1 to 2.25 MPa. The range between the initial and final stress, the stress range, had an average of 0.19 ± 0.3.

The equations in the METHODOLOGY section were used to determine the magnitude of the final stress at failure. The S-N curve in Figure 16 and Figure 17 is the calculated final stress plotted against the Number of Cycles to Failure, N, and Log(N). The final stress was also normalized to the ultimate strength of the adjacent sample. The % S-N and % S-Log(N) curve is plotted in Figure 18 and Figure 19. Both the S-Log(N) and the Normalized S-Log(N) show the trend of the fatigue life increasing as the magnitude of stress decreases.

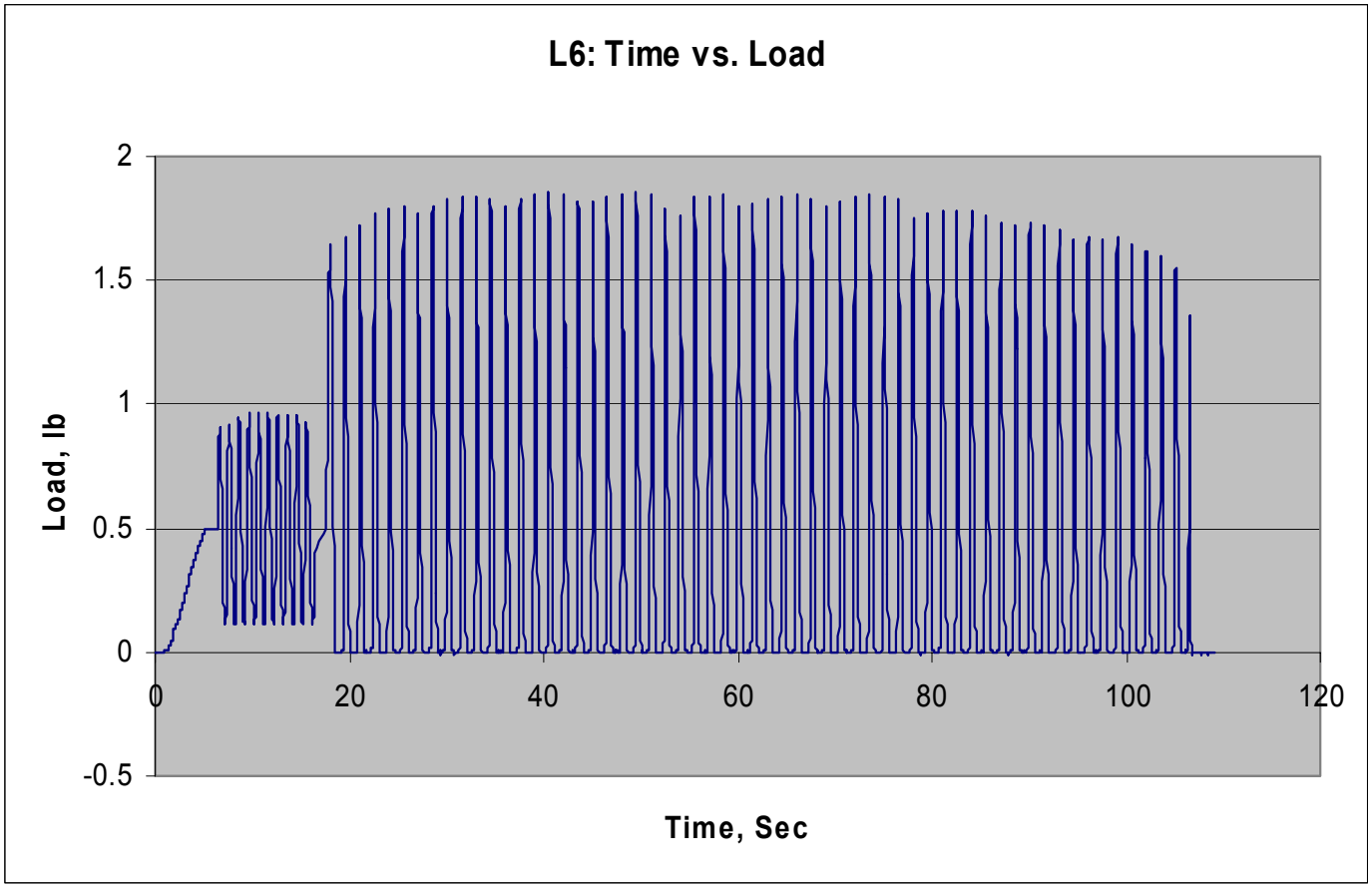

Figure 10: Artery L6 Cyclic Fatigue Test

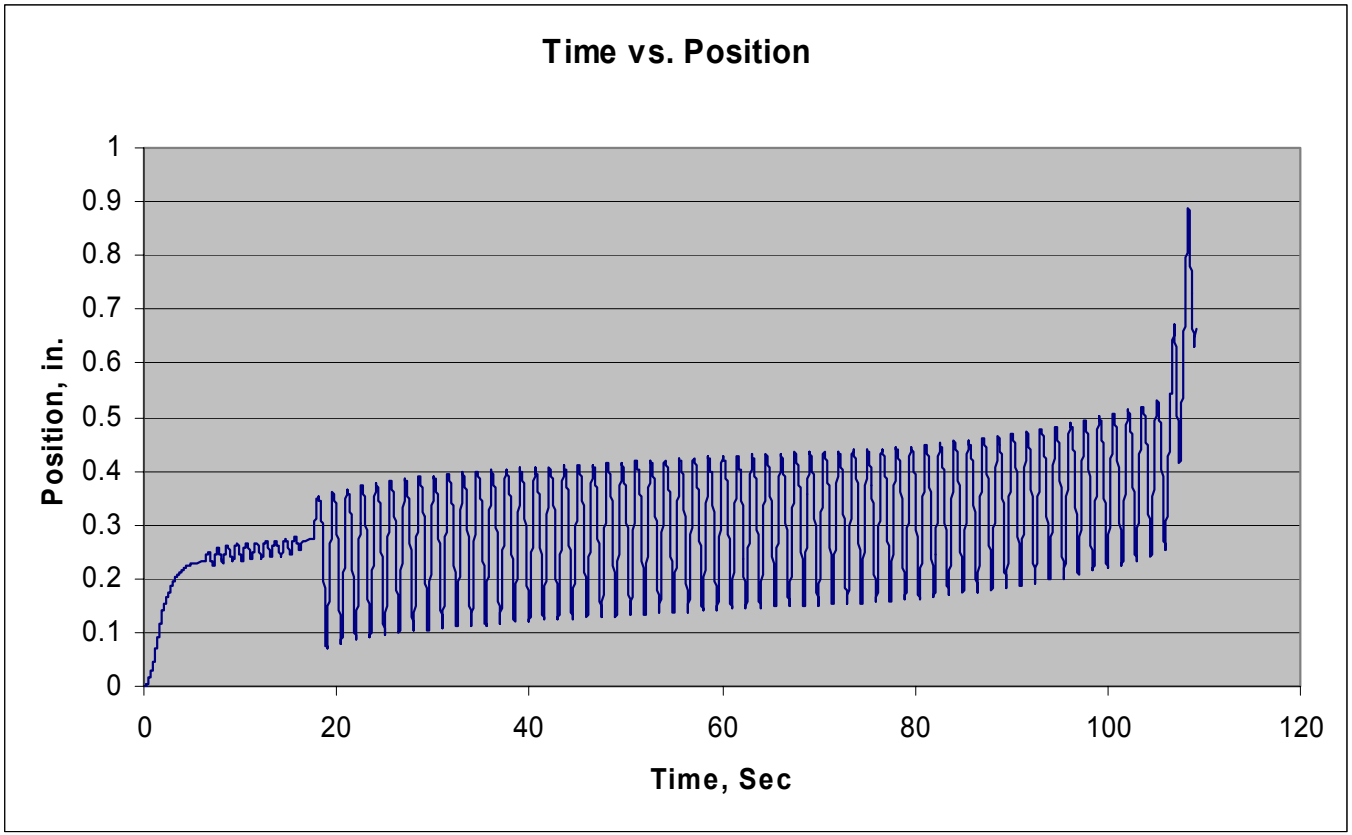

Figure 11: Artery L6 Cyclic Fatigue Test

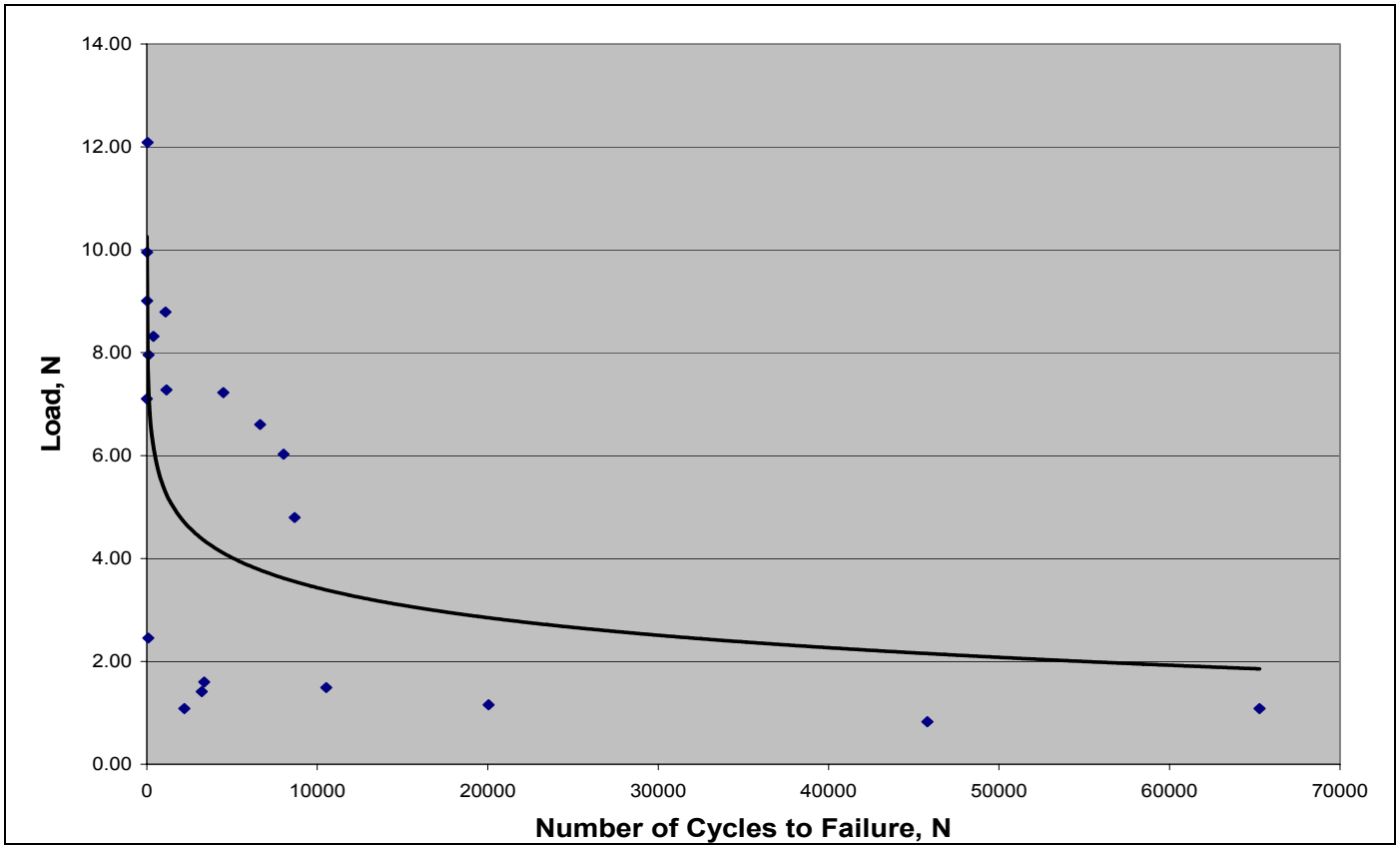

Figure 12: Load-N Curve

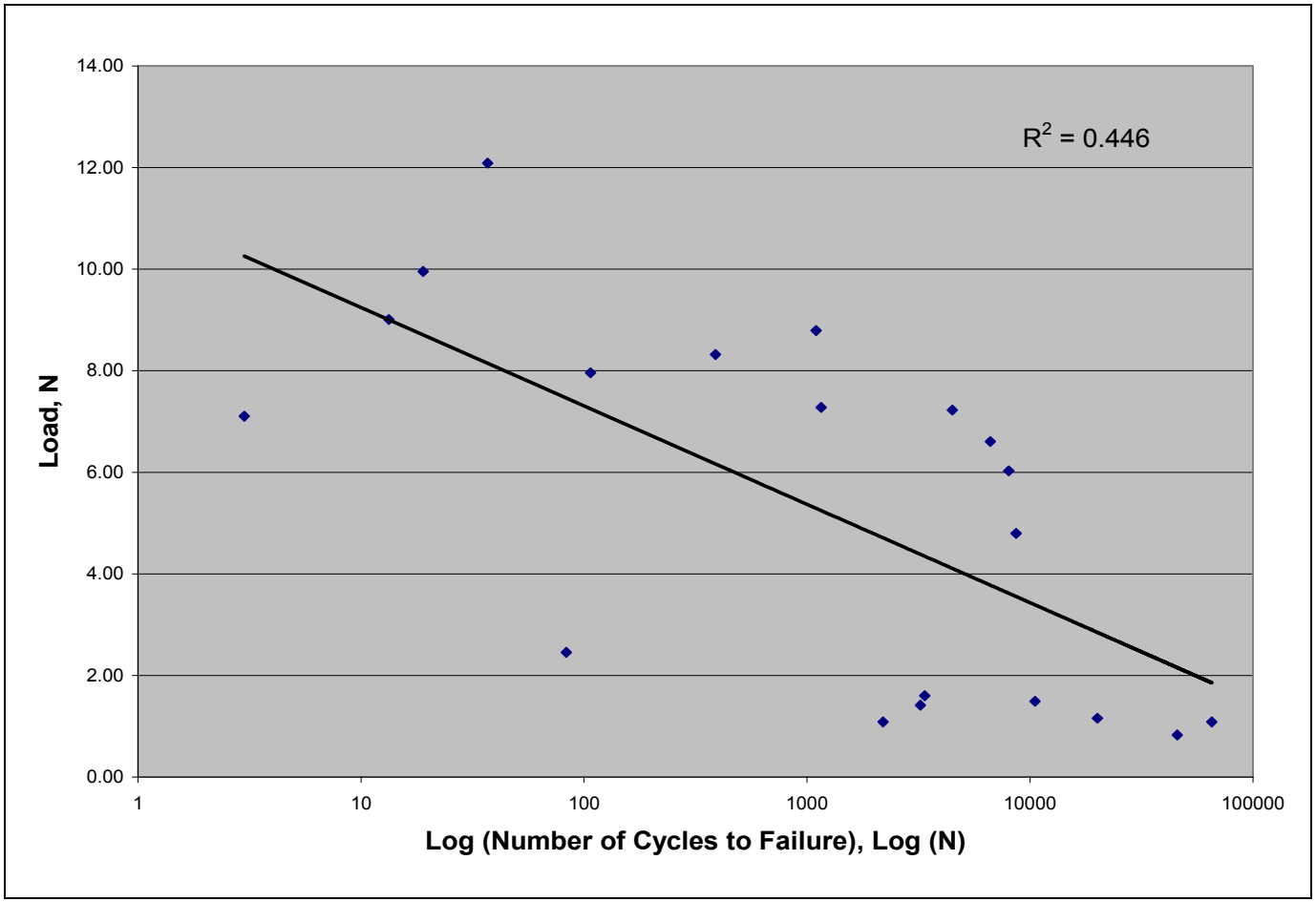

Figure 13: Load-Log(N)

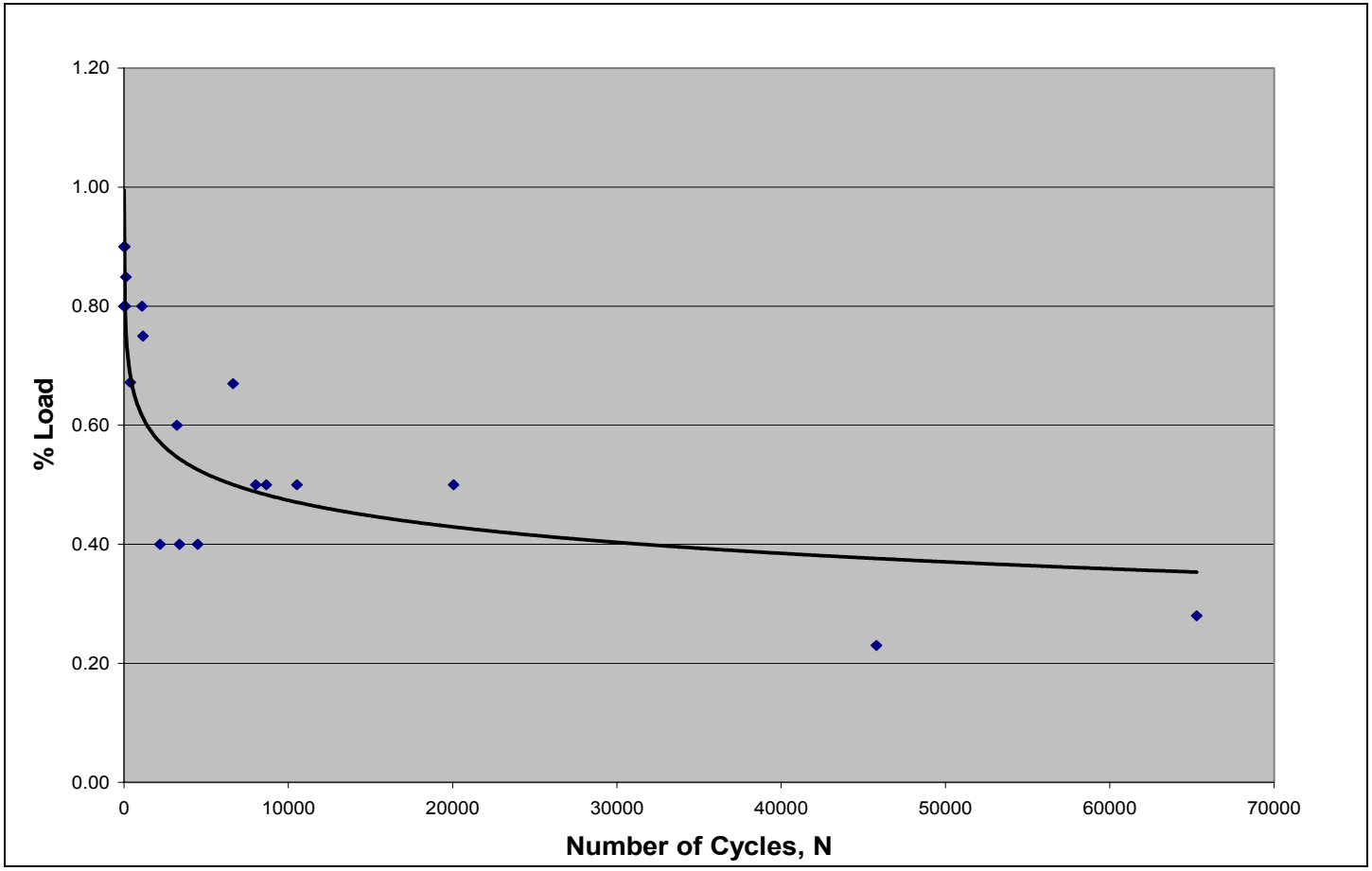

Figure 14: N vs. % Load

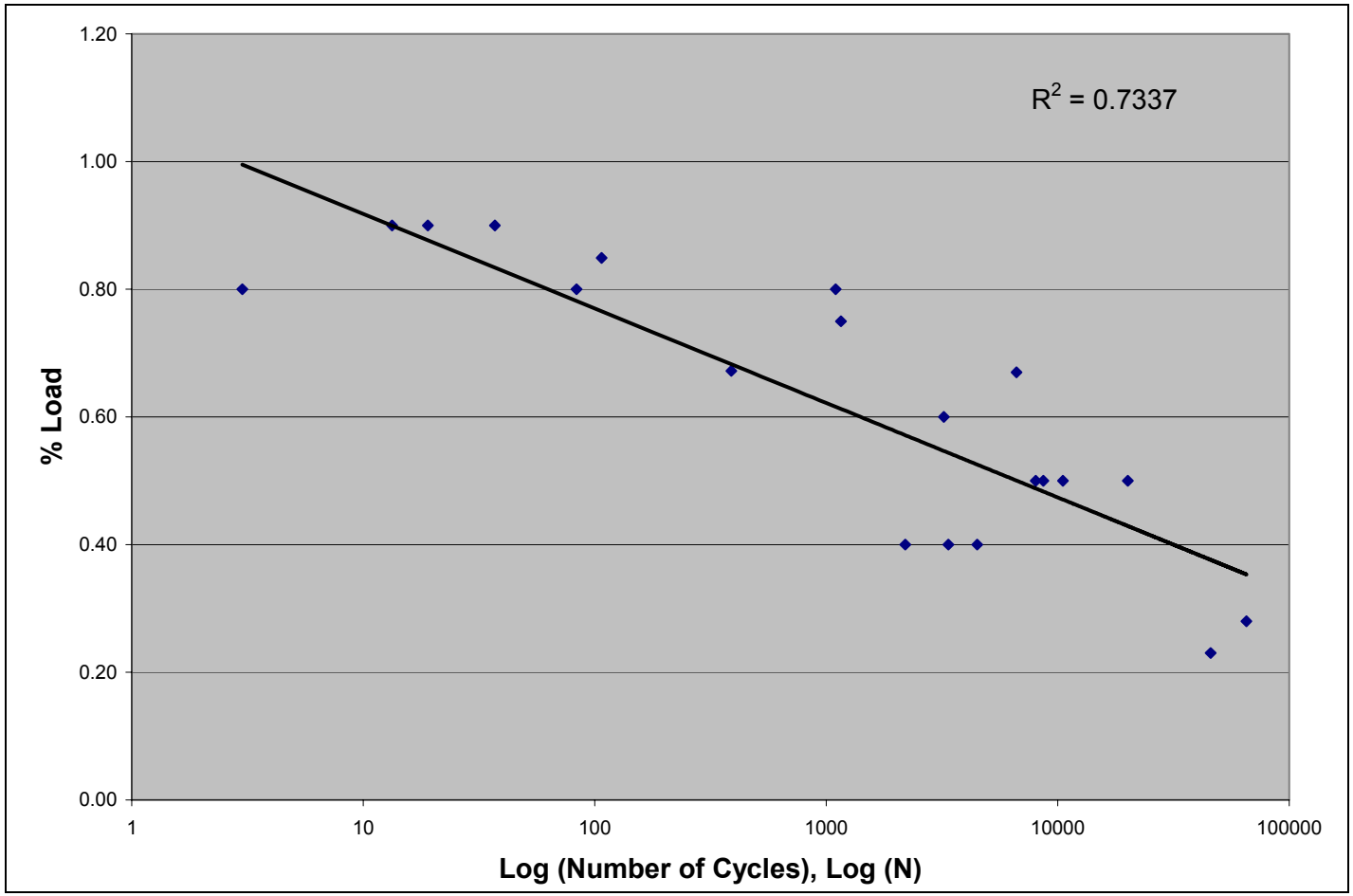

Figure 15: Log (N) vs. % Load

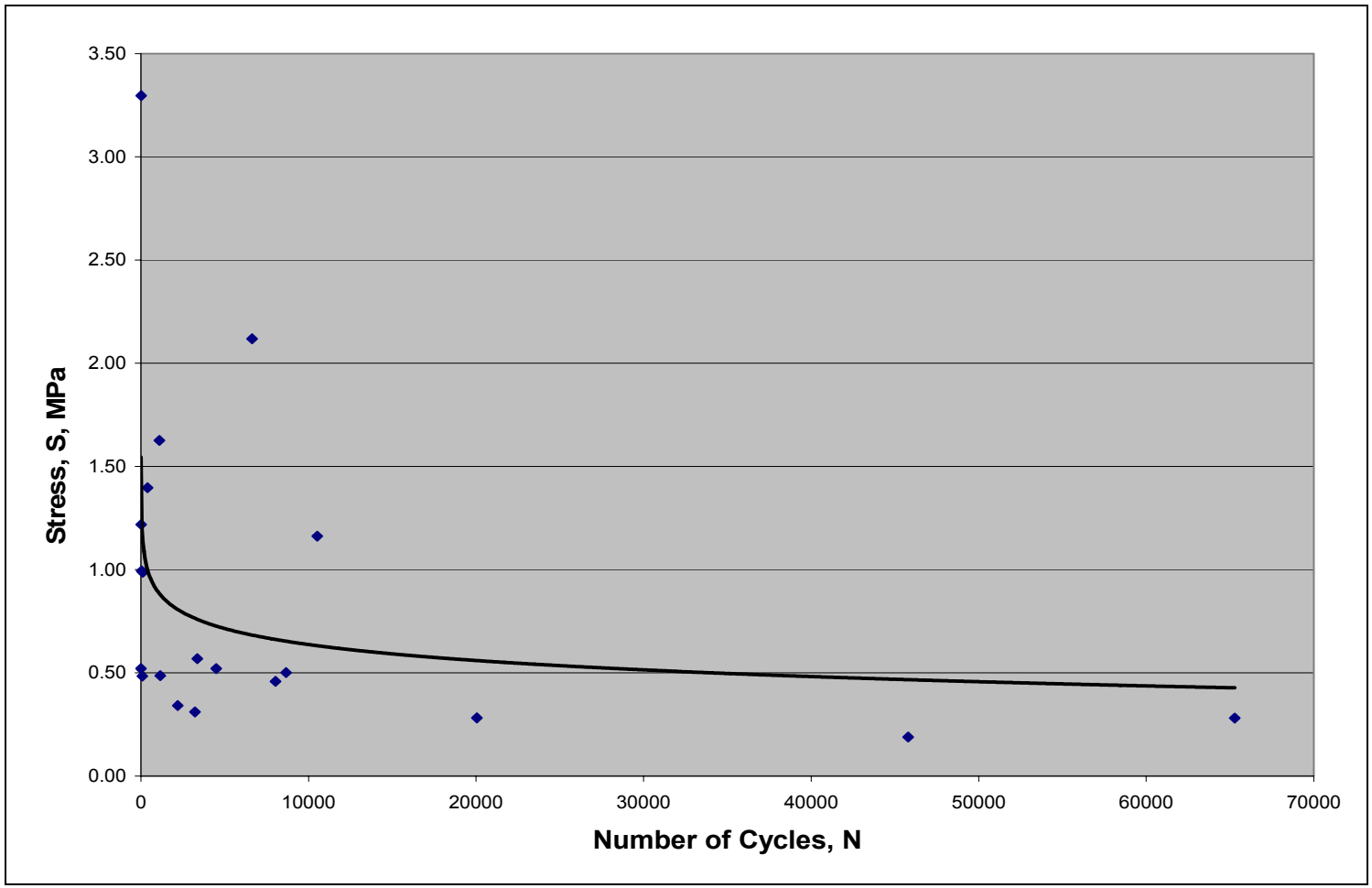

Figure 16: S-N Curve

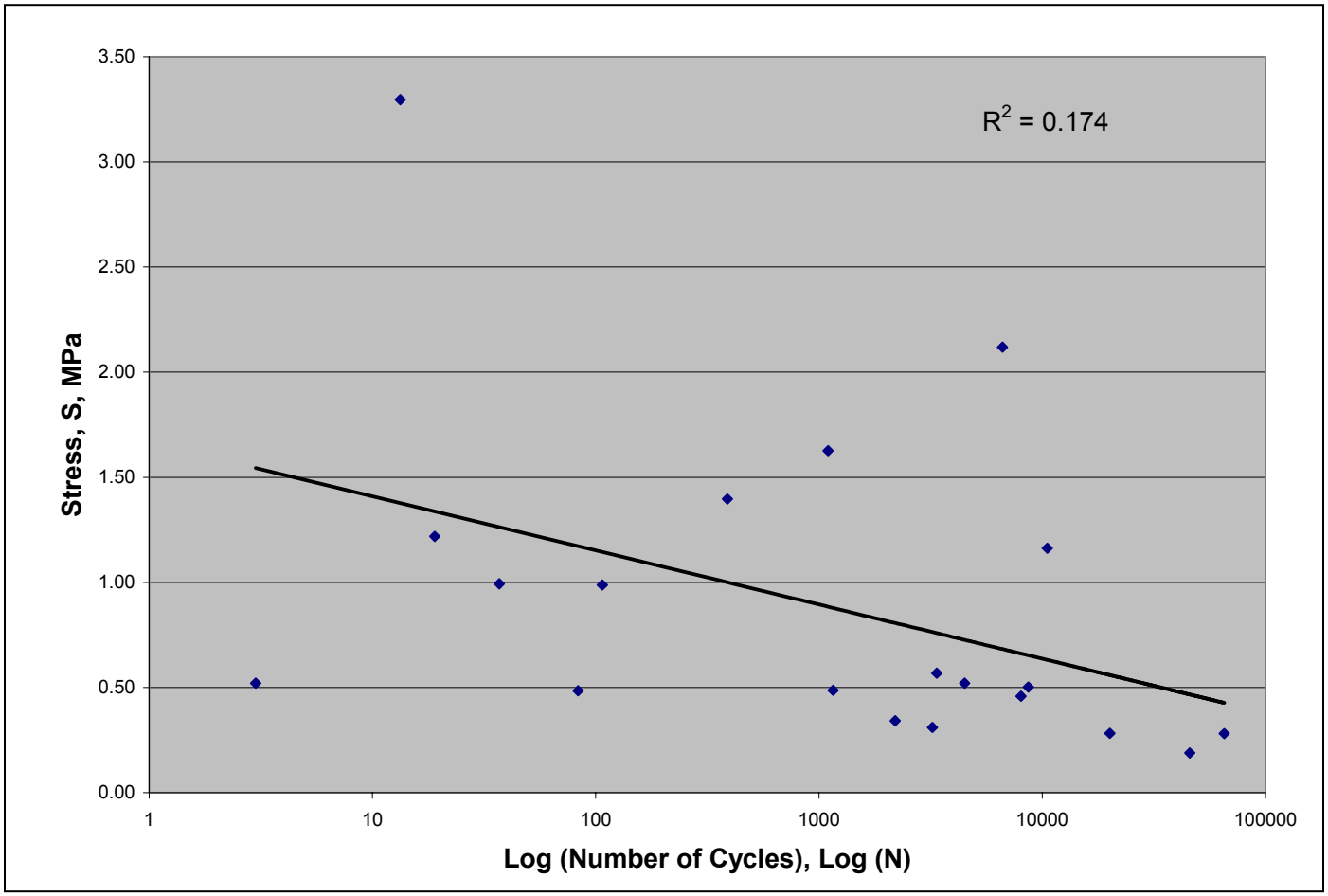

Figure 17: S-Log(N)

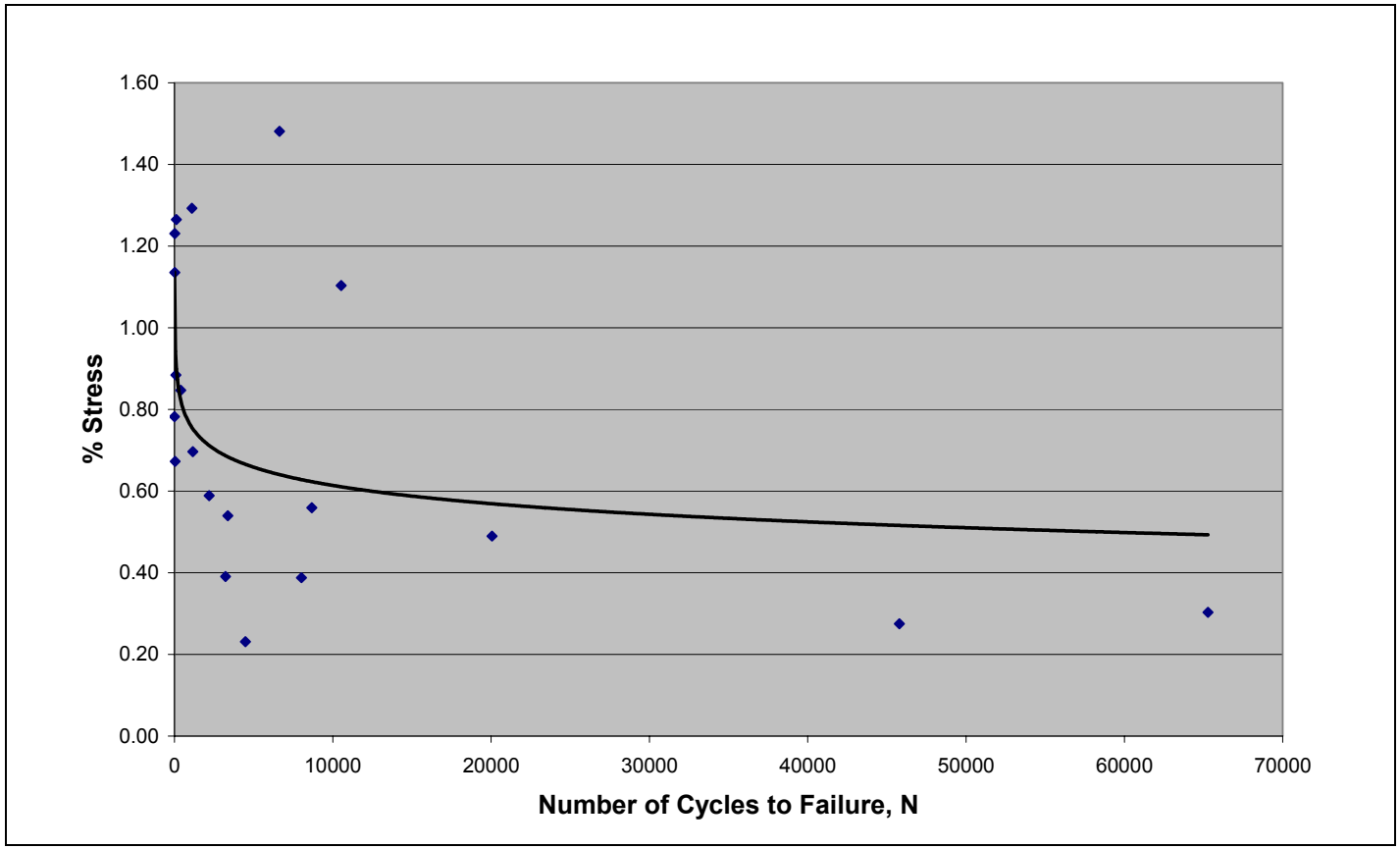

Figure 18: % S- N Curve

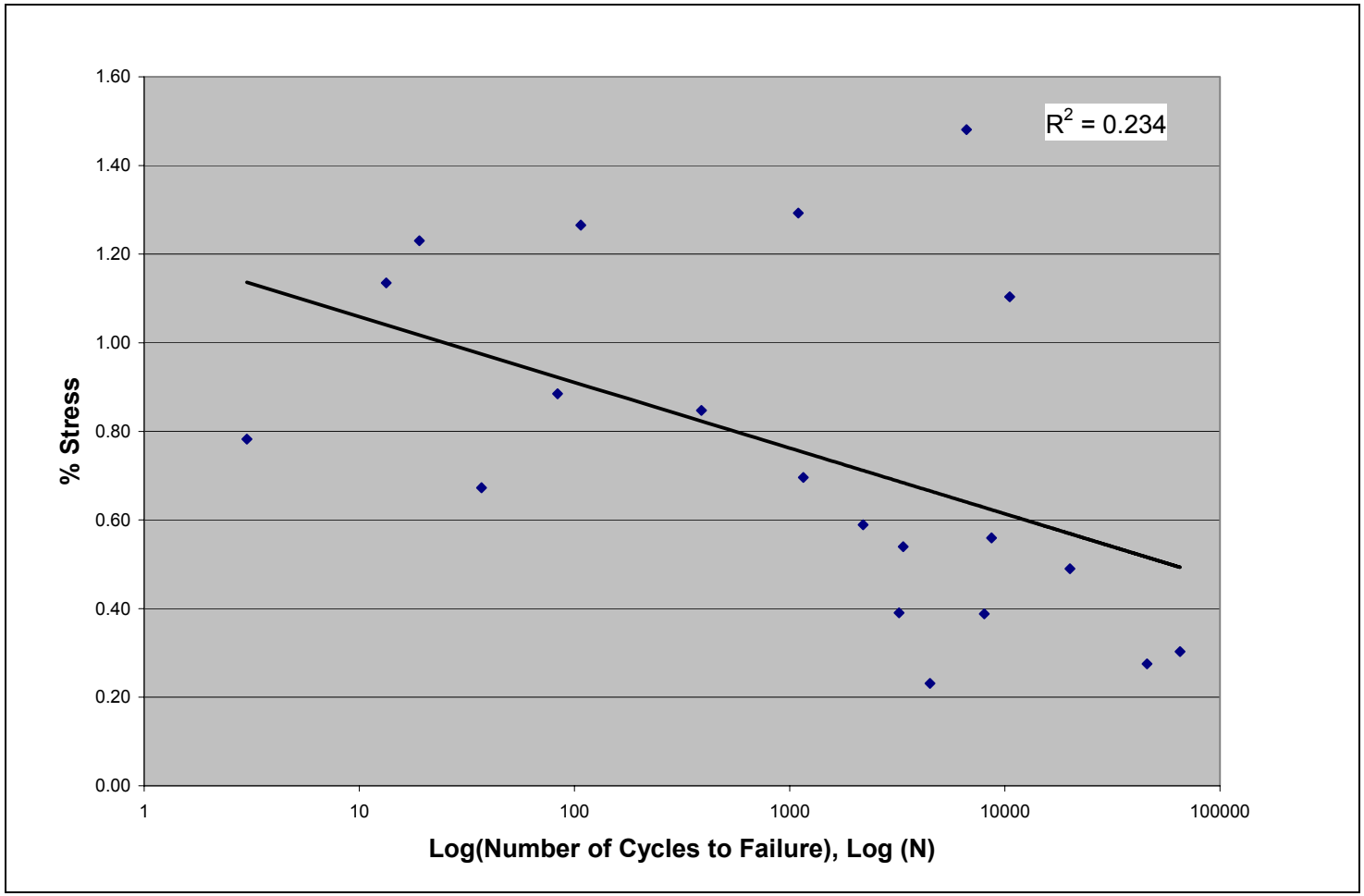

Figure 19: % S-Log(N) Curve

Histology

Histological samples were examined from a control sample, a sample that was cycled, and a sample that was pulled in tension to failure. The control sample was not subjected to any loading or testing. The control image shows the three layer structure of the artery, the waviness of the collagen fibers and straight elastin fibers. The layers of the control specimen appear very ordered.

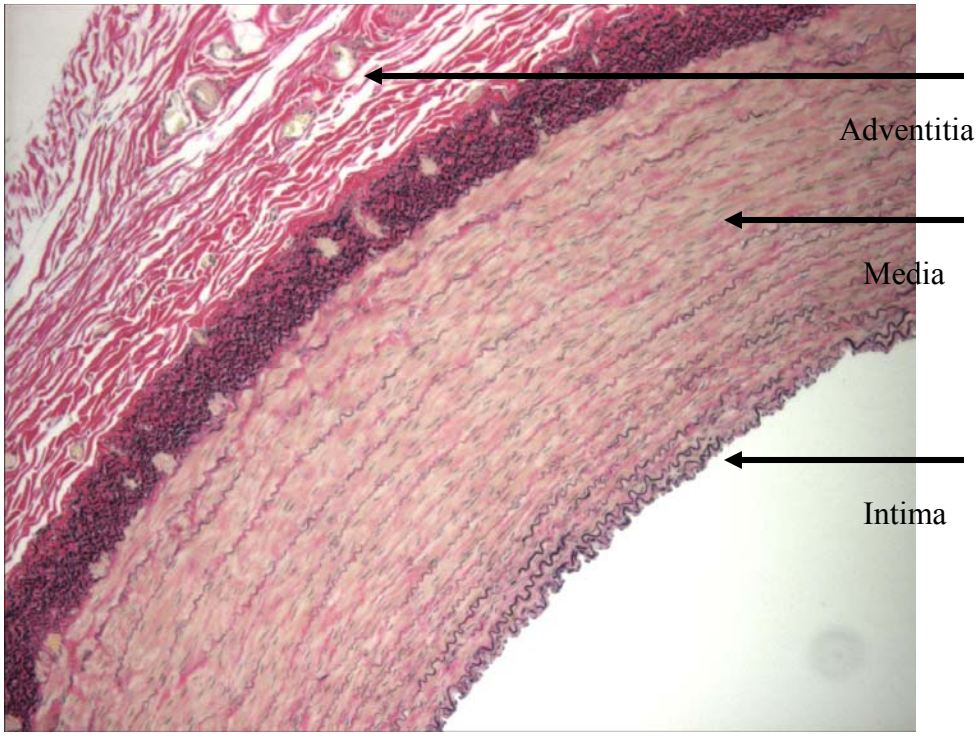

Figure 20: Histological stain of a control artery.
Collagen is stained pink and Elastin is stained black

After cycling the components in the artery layers are much less ordered. It is also possible to see areas within the medial layer where the collagen is separating due to

fatigue damage. The arrows in Figure 21 show the areas of damage that is occurring as circumferential tears in the media. The tears are appearing about 2/3 into the depth of the media layer. Figure 22 shows a higher magnification of the circled damage in Figure 21. The damage does not appear to be accumulating in the adventitial layer, nor are there radial tears evident.

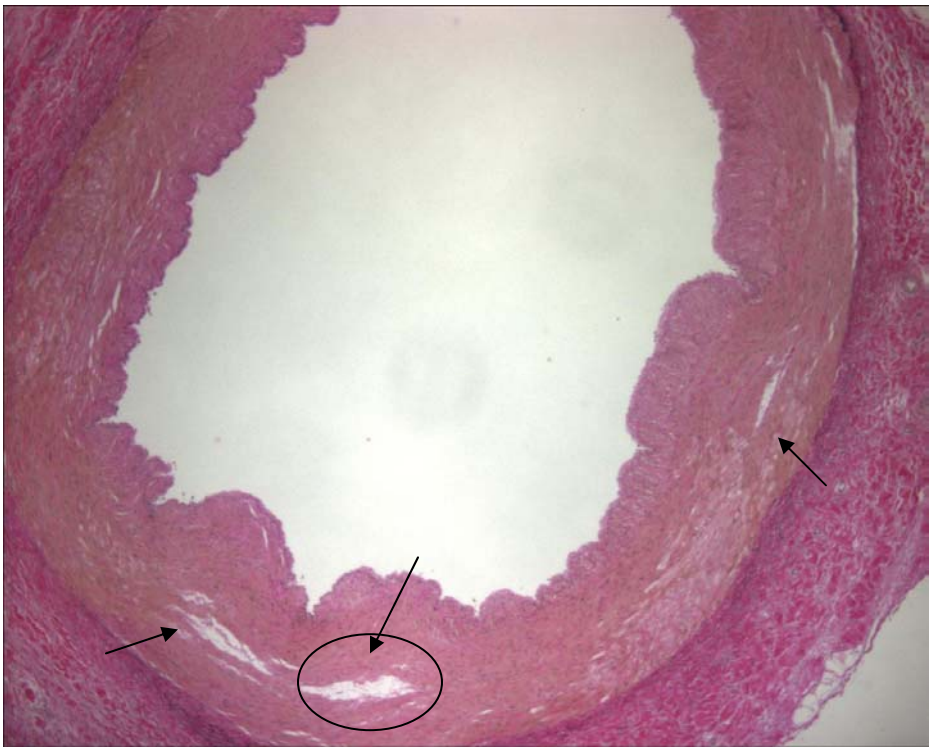

Figure 21: Cycled Artery exhibiting fatigue damage

The arrows point out the areas of visible damage, 4x magnification. The section pointed to by the middle arrow is enlarged in Figure 22 below.

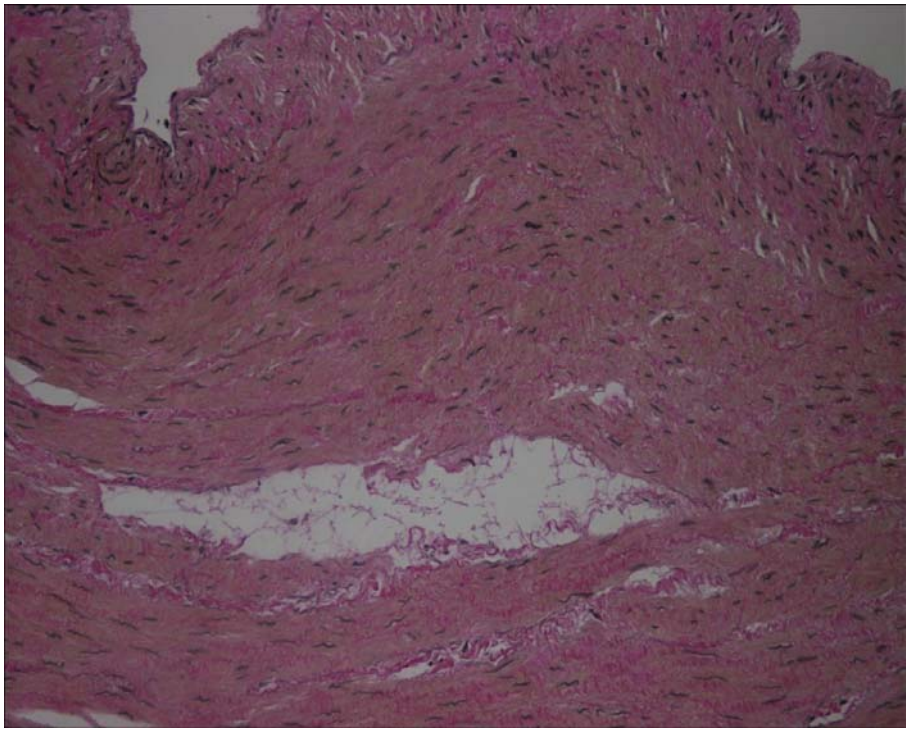

Figure 22: 20x magnification of a section of damage in the cycled artery

The ultimate strength tests exhibit the most damage to the tissue as can be seen in Figure 23 and Figure 24. The tears at the end of the segments are jagged and the layers are less organized than the control.

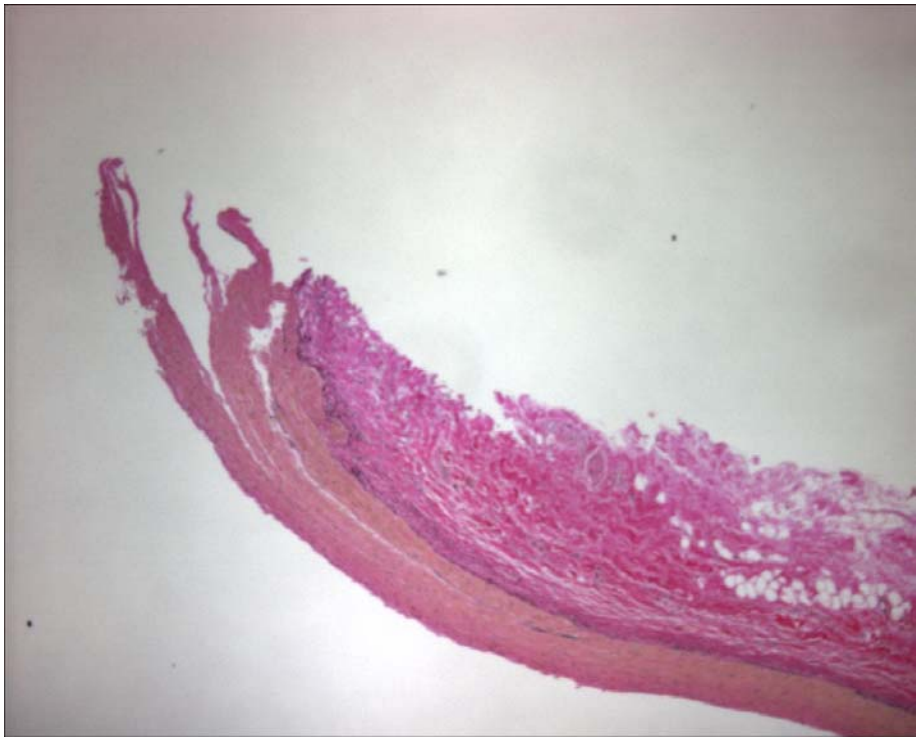

Figure 23: One end of sample after an ultimate tensile test

One end of torn media and adventitia after an ultimate tensile strength test, 4x magnification

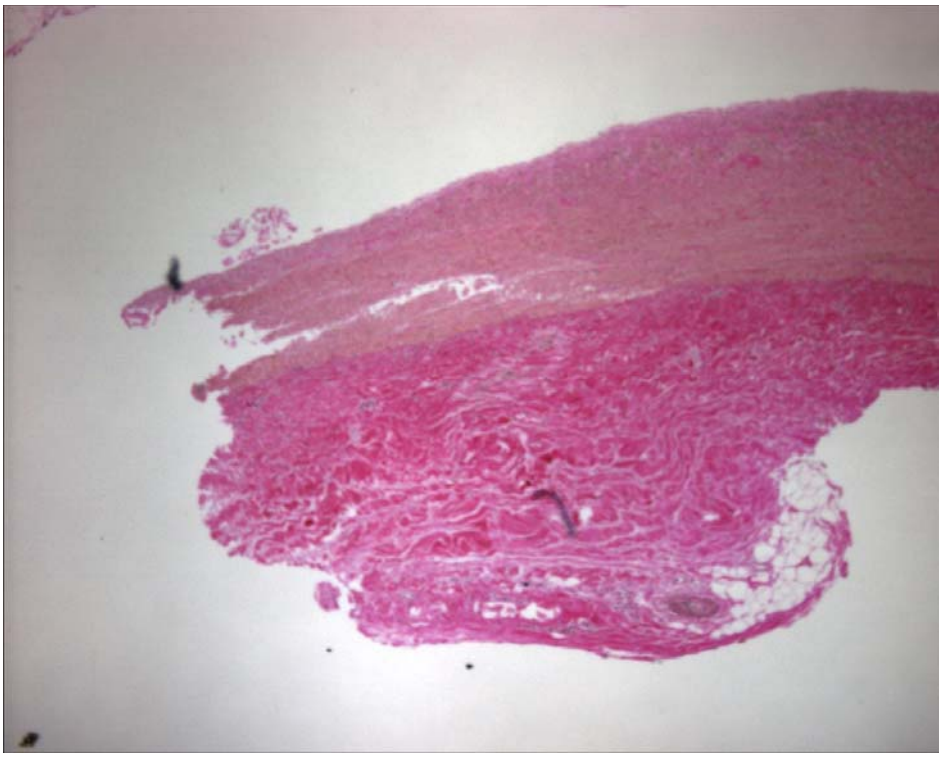

Figure 24: The other end of the sample after an ultimate tensile test

Torn media and adventitia shown in Figure 23, after an ultimate tensile test, 4x magnification

The histological pictures show that the nature of the damage to the arterial wall as the sample is cycled. The differences between the control and the cycled sample is that the components of the layers become more disorganized with cycling, and the cycled wall shows areas of delamination, where the collagen is separating (Figure 22).

CHAPTER 4

DISCUSSION

This work has determined a range for the ultimate strength of porcine arteries and has quantified a trend in the fatigue failure behavior of the artery. Also in this work histological changes at during a pull test and a long cyclic test were compared to a control specimen.

Artery samples were mounted on hooks and pulled to failure using a load controlled servo-electromechanical testing machine. The final or ultimate load, at sample failure, was used to calculate the maximum stress experienced by the artery wall. The Ultimate Load values ranged from 2.31 N (0.52 lb.) to 25.27 N (5.68 lb.). The average ultimate load at failure was 9.91 $\pm$ 5.76 N. 90% of the Ultimate loads were between 2.31 and 9.71 N, 50% between 2.31 and 14.94 N.

The Ultimate Strength measurements ranged from 0.55 (1170 mmHg) to 2.55 MPa (12341 mmHg), with an average of 1.48 $\pm$ 0.49 MPa (4023 $\pm$ 2350 mmHg). 100% of the pulled samples failed, 90% of them failing within a stress range of 0.57 to 1.89 MPa and 50% failing within 0.7 and 1.41 MPa. Only two of the samples (5.8%) failed at stresses above 2 MPa.

The position measurements that were recorded during testing were used to determine the stretch ratio, final circumference/initial circumference, of the samples. The stretch ratios for the Ultimate Strength tests averaged 2.06 $\pm$ 0.63.depending on the amount of displacement required to fail the sample. Since failure was defined as a complete tear of all tissue across the specimen wall, the stretch ratios may be affected by excess connective tissue on the outside of the artery. This excess connective tissue may

have taken more displacement than the artery wall before failing, so the artery wall may have failed although it was not clearly evident due to the surrounding intact connective tissue. This may have increased the final position measurement and therefore the stretch ratio. However, even with this possible error the average stretch ratio is 2.06 ± 0.63.

For the cyclic fatigue tests, artery samples were cycled at a constant load. The constant load was set at a percentage of the ultimate load measured from an adjacent sample. The total Number of Cycles to Failure ranged from 3 to 65,280. The relationships between the Load, % Load, Stress, and % Stress vs. the Number of Cycles to Failure were evaluated. The correlation coefficient, r, for each relationship was determined. The correlation coefficient is a statistical value that expresses the strength of the linear relationship between two variables [44]. The r values for % Stress vs. Log(N) and Stress vs. Log (N) were 0.484 and 0.417 respectively. These correlation coefficients are not statistically significant ($r>0.8$ for statistical significance) and this is due to variability of biological tissue. The % Stress correlation coefficient is better than the Stress correlation because the % Stress is normalized to the adjacent sample. The r-values of the Load and % Load vs. Log(N) were 0.668 and 0.856 respectively. The correlation coefficient of $r=0.856$ for the % Load vs. N is statistically significant. This correlation coefficient indicates a strong relationship between the %load and the Number of Cycles to Failure. The other relationships, though not statistically significant, all show a negative slope, indicating that plastic deformation is taking place; a flat curve would indicate the material was exhibiting no fatigue damage accumulation.

The testing was performed on adjacent pairs of artery samples due to heterogeneity of the artery. S-N curves are based on tests at constant stresses that are

below the ultimate strength of the material. Since the mechanical properties, and therefore the ultimate strength values, change along the length of the artery it was necessary to determine the ultimate strength for each pair before setting the magnitude of the constant cyclic load. This process ensured that a load was selected below the ultimate strength of the material. However, in 6 cases (Artery samples L4, L6, R2, R4, P3, T8) although the load was set below the ultimate load of the material the final stress at failure was higher than the stress required to break the adjacent sample in tension. This discrepancy is due to human error in the measurements of the specimen. Since the initial area measurement is part of the equation for calculating the final stress, errors in the measurement will greatly affect the stress value calculated. The measurements were done using electronic calipers and it is possible that forces applied to the specimen with the calipers could have caused some errors in the recorded values. In order to reduce the amount of measurement error, the measurements were taken in triplicate and averaged for use in calculations. Another factor that affected the stress calculation is the stretch ratio. Specimen that cycled to failure at higher stresses than the ultimate strength of the adjacent specimen had higher stretch ratios than the adjacent specimen. This larger stretch ratio, due to a large amount of stretch experienced by the circumference, increased the stress value and in these cases resulted in a normalized stress >1.

The accumulation of damage shown by histology indicates that fatigue damage is accumulating and the positive slope of the time vs. position curve indicates that the material will fail. The correlation between the % Load and the Number of Cycles to failure allows for an estimation of the Number of Cycles to Failure. Therefore, the fatigue failure point of soft tissue can be predicted.

Comparison To Previous Research

Aortic Tissue

Uniaxial tensile tests performed on strips of aortic tissue by Okamoto et al. determined an ultimate strength range of 1.35 $\pm$ 0.37 MPa to 2.40 $\pm$ 0.46 MPa depending on the age of the specimen [45]. Haut [38]performed uniaxial tests on ring specimen from the aorta and found an average ultimate strength of 1.891 $\pm$ 0.256 MPa. Mohan and Melvin [12]also performed uniaxial tests on strips of aortic tissue, reporting an average ultimate strength of 147 $\pm$ 91 N/m^2 (1.47 $\pm$ 0.91 MPa) and an average strain ratio of 1.47 $\pm$ 0.23. These values are higher than the average of 0.89 $\pm$ 0.77 MPa found for the coronary arteries in this work. The aorta is a large (conducting) artery, and the difference in size and structure from the smaller coronary artery explains why the values at failure determined in this work are lower than the failure stresses found for the aorta.

Plaque Caps

Lendon et al. (1991) [21] performed tensile tests on strips of atherosclerotic plaque caps and found the maximum tensile stress to be within the range of 0.5 to 0.7 MPa. These values fell within the range that the same research group had previously published for the tensile strength of plaque caps, 0.012 to 1.938 MPa [46]. The ultimate strength values in this work are slightly higher than former range determined by Lendon et al. for the atherosclerotic plaques. This difference is expected since the plaques, though similar in composition, do not have the same three layer structure of the arterial wall.

Cheng et al. [16] researched the rupture of plaques in regions of high tensile circumferential stress. They found that the circumferential stress in plaques that rupture are higher than the stresses in stable plaques. The maximum circumferential stress for ruptured plaques was 4,091 $\pm$ 1,199 mmHg and 1,444 $\pm$ 485 mmHg for stable plaques. They also determined that it is unusual for atherosclerotic tissue to fracture at stresses less than 300 kPa (2,250 mmHg) [16]. The estimated pressure values calculated in the present work were, 3814 $\pm$ 2214 mmHg (0.5 $\pm$ 0.3 MPa) and 2394 $\pm$ 1292 mmHg (0.3 $\pm$ 0.2 MPa), for the ultimate strength and cyclic tests respectively. The overall maximum pressure was 12,341 mmHg (2.77 MPa) and the overall minimum was 627 mmHg (0.19 MPa), both of which occurred in cyclic tests. These values are also comparable with the burst pressure of porcine arteries of 3100 mmHg measured by Chin Quee[47]. The pressure value from the ultimate strength test is comparable to the circumferential stress for the stable lesion, and it is higher due to differences in structure.

Tendon and Ligaments

Ultimate strengths have been established for soft tissue such as tendon and ligaments. Johnson et al. researched the tensile and viscoelastic properties of human patellar tendon and determined ultimate strength values of 64.7 $\pm$ 15.0 MPa [36]. In work by Quapp and Weiss they found that human medial collateral ligaments have ultimate strength values of 38.56 $\pm$ 4.76 MPa in the longitudinal direction and 1.69 $\pm$ 0.53 MPa in the transverse direction [34]. These values are much larger than those found in this research because of the differences in structure. Tendon and ligaments are made of parallel collagen fibers, as opposed to the complex three-dimensional structure of blood

vessels. Collagen has an ultimate strength of 50-100 MPa [6]. The ultimate strain values of tendon and ligament were 14 $\pm$ 6% [36] and 17.11 $\pm$ 1.53% [34], respectively.

Sclera

Time vs. position data was recorded while the cyclic tests were performed. This data, plotted in Figure 11, has a positive slope of about 0.6 mm/sec. The positive slope of the time vs. position curve is similar to that found by Ku and Greene [5]. They identified this trend with a cyclic test on rabbit sclera. This trend indicates that the material is weakened as it is being cycled and that it will eventually fail. Since the primary structural components of the artery are collagen and elastin, this gradual weakening would affect these two components. However, collagen and elastin have different mechanical properties and may fatigue and fail at different points. This leads to a model of failure that is similar to one suggested by Eli Altus for the evolution of fatigue damage [48]. Altus' model states that as a material is cycled at a constant load, weak elements of the material will break first. As the weak elements break local stress concentrations are formed leading to higher or lower strains on the neighboring elements. This process is termed the *cyclic damage progression effect*. It is proposed by this work that the cyclic damage progression effect accumulates in the arterial wall among the collagen and elastin elements, as demonstrated by the positive slope of the time vs. position curve, eventually leading to failure of the material. The failure of the collagen and elastin components can be seen with histology.

Limitations

The outcome of experiments is affected by the methodology. Experimental error that may have occurred in this work is discussed in the following paragraphs.

Soft Tissues

Biological tissues have a large amount of variability. Therefore one of the greatest limitations of these experiments is biological variability. Another issue with tissue is the availability of human arteries for testing. Porcine arteries are used in this work because they are structurally similar to human arteries and they are easy to obtain. It has been discovered by [30] that porcine arteries are more elastic than human arteries, however this is expected in testing because human arteries are generally from older patients who likely have some degree of atherosclerotic disease, whereas porcine arteries are harvested from young healthy (non-diseased) animals. Furthermore, the fatigue of arteries affects the collagen and elastin structures so any work that leads to a greater understanding of how the components fatigue will help in understanding the behavior of the whole tissue.

Sample Preparation and Test Setup

The ring samples were cut from the artery length by hand. The cuts were made using a razor blade so that only one cut was necessary to separate the ring. However the misalignment of the razor may have caused cuts that were not straight. This affected ring measurements and possibly changed the distribution of stress.

The dimension measurements, taken by hand, of the arterial samples are a limitation to the accuracy of this work because it is possible that forces applied to the

specimen affected the recorded measurements. However, great care was taken to minimize the amount of deformation of the artery and measurements were taken in triplicate and averaged to compensate for error. Measurements of the dimensions and the force were also affected by excess connective tissue. Connective tissue was removed by hand to as great an extent as possible, however tissue that was unable to be removed potentially increased outer diameter measurements. Although it is not expected that the connective tissue provides a great amount of mechanical strength, it may have affected the loading of the material to failure since additional tissue on the outside of the artery wall had to be broken.

Testing was performed in a bath of PBS, which is used to maintain the mechanical properties of the tissue by preventing it from drying out. However, in this work the solution was maintained at room temperature (24ºC) rather than body temperature (37ºC). It is unknown how the temperature difference may affect the behavior of the tissue. The hooks used to hold the rings for testing had a circular cross-section. The circular cross-section was chosen to reduce the effects of stress concentrations that could occur with sharp edges (i.e. a square cross-section),

Constant Load vs. Constant Stress

For the fatigue tests performed in this work the load was held constant rather than the stress because the stress changes as the area of the specimen decreases over time. The equations used for the calculation of stress are well developed in the field for uniaxial tests [9, 31], and adequately define the final stress. In this work the final stress was assumed to be the cyclic stress of the material, although the magnitude of stress is actually changing with time as the cross-sectional area decreases.

The change in the cross-sectional area posed an additional limitation during testing. As the specimen was loaded to failure, the thickness on one side of the ring sample decreased at a higher rate than the other side, resulting in a higher rate of decreased cross-sectional area. Stress is a function of the cross sectional area. Therefore, one side of the sample experienced higher stresses than the other side. The uneven distribution of stress in the sample was not accounted for.

Clinical Significance

All of the samples in this work broke at stresses between 0.5 MPa (1170 mmHg) and 2.5 MPa (12341 mmHg). The stress in arterial walls can be estimated if the blood pressure is known, and therefore rupture can be predicted if the stress in the wall is within this range or determined to be higher than 2.5 MPa. Knowing a range for the ultimate strength value, and thus point of rupture, provides a diagnostic tool that has not been previously defined. Determining the ultimate strength of healthy arteries also provides a basis to compare the changes in arteries from effects such as diet, drug related or mechanical intervention.

It is well known that materials fatigue when subjected to repeated loading. This occurs everyday in materials such as metals and composites, and it also occurs in our bodies. Cyclic pressure applied to the sclera of the eye, from actions such as hard squinting or rubbing, causes irreversible lengthening of the eyeball leading to the condition of myopia [5]. It is hypothesized in this work that the primary structural components of the artery, collagen and elastin, fatigue and eventually lead to failure of

the arterial wall. *In vivo* collagen is regenerated, but elastin is regenerated at a nearly negligible rate. Therefore, as elastin is fatigued and eventually fails, the collagen fibers will be required to carry more of the load. The cycling of collagen under the increased load will fatigue the fibers, most likely at an accelerated rate, and eventually lead to complete failure.

Complete failure was demonstrated in this work and indicates the trend of decreasing strength with an increased number of cycles. Rupture of the artery occurs in different forms and affects many lives each year. Common arterial ruptures are rupture of the pulmonary, abdominal aortic rupture and the rupture of atherosclerotic plaque caps. These ruptures occur in different locations in the body, but their common feature is that they are unpredictable. The data collected from the fatigue experiments performed in the current work were collected and plotted as S-N and %Load-N curves. These curves are critical for clinical application because they allow the failure point of the artery to be predicted based on the stress at which the artery is being cycled. The stress within the arterial wall can be determined by the local blood pressure, which may be affected by factors such as stenosis within the vessel. Knowing this stress, the Number of Cycles to Failure can be predicted. Although the number of cycles will not be exact, a range of estimated time is better than no estimate leading to events such as Sudden Cardiac Death. The data collected is also significant for aneurysms because the walls are thinner and therefore may experiences higher stresses from normal cyclic loads due to a smaller cross-sectional area. Knowing the S-N behavior could help predict when the aneurysm, being subjected to potentially higher than normal stresses, will fail.

The heart beats over 33 million times per year. The Number of Cycles to Failure for samples cycled at 0.28 MPa (1013 mmHg) was 65,280. This cyclic test was based on 28% of the ultimate load. Although 1013 mmHg is a higher pressure than those found in the body, it could be predicted from the % Load vs. N curve that if the pressure in the body reaches 300 mmHg, the resulting pressure based on a cyclic test at 4% of the ultimate load, then the Number of Cycles to Failure will be on the order of 8 million cycles. This number of cycles occurs within three months.

Future Work

This research has determined a range for the Ultimate Strength and a trend in the fatigue behavior of porcine arteries. The ultimate strength values were calculated from tensile tests on ring specimen and the fatigue behavior is demonstrated on S-N and %Load-N curves.

To further corroborate the findings of this work it is suggested that more fatigue tests be performed on porcine arteries. After establishing a more robust S-N curve, the fatigue tests could be extended to human arteries and if possible atherosclerotic plaque caps. To achieve results that better represent *in vivo* loading, tests should be performed on cylindrical arterial samples that are cyclically pressurized.

This work is useful for predicting the Number of Cycles to Failure of a patient's artery, based on the cyclic stress being experienced. However, in order to better prevent the artery from actually failing it is necessary to understand how the material fails. The primary structural components are collagen and elastin so it would be useful to use

histology to observe the changes in these components during cycling. Using an established S-N curve one can better predict the failure of the artery and can therefore determine points during the test to stop and study the histological changes.

CHAPTER 5

CONCLUSIONS

In this work tests were performed to determine the ultimate strength and fatigue behavior of porcine coronary arteries. The ultimate strength tests were performed on ring specimen that were pulled to failure in a tensile load controlled test. The cyclic fatigue tests were performed on ring specimen that were 3-5 mm in width, and were cycled to failure at a load below the ultimate load of a neighboring sample.

The ultimate strength results were in the range of 0.46 to 2.55 MPa. This range is similar to those found in previous work on aortic tissue (1.35 $\pm$ 0.37 MPa to 2.40 $\pm$ 0.46 MPa) and human plaque caps (0.012 to 1.938 MPa). The burst pressures found in this work (3814 $\pm$ 2214 mmHg) also agree with those found in previous work (3100 mmHg).

The cyclic fatigue tests produced a strong correlation, r=0.856, between the %Load and the Log (Number of Cycles to Failure). The Position vs. Time data that was collected during testing had a positive slope. This positive slope, which can be seen very early in testing indicates if the material will fail or not. Therefore, within the first few minutes of testing it is possible to know if the material is going to fail. The point of failure can be predicted by the relationship between the %Load and Number of Cycles to Failure. Histology further confirmed the fatigue failure of the artery. The damage in the artery before the sample had failed indicated damage accumulation due to the cyclic fatigue process.

In conclusion, this work provides a range of values for the ultimate load of

arteries and a relationship between the fatigue failure of arteries and the % Load that it is cycled at. The results suggest that the fatigue failure point of coronary artery tissue and aneurysms can be predicted.

APPENDIX A: DEFORMATION OF A TUBULAR SPECIMEN

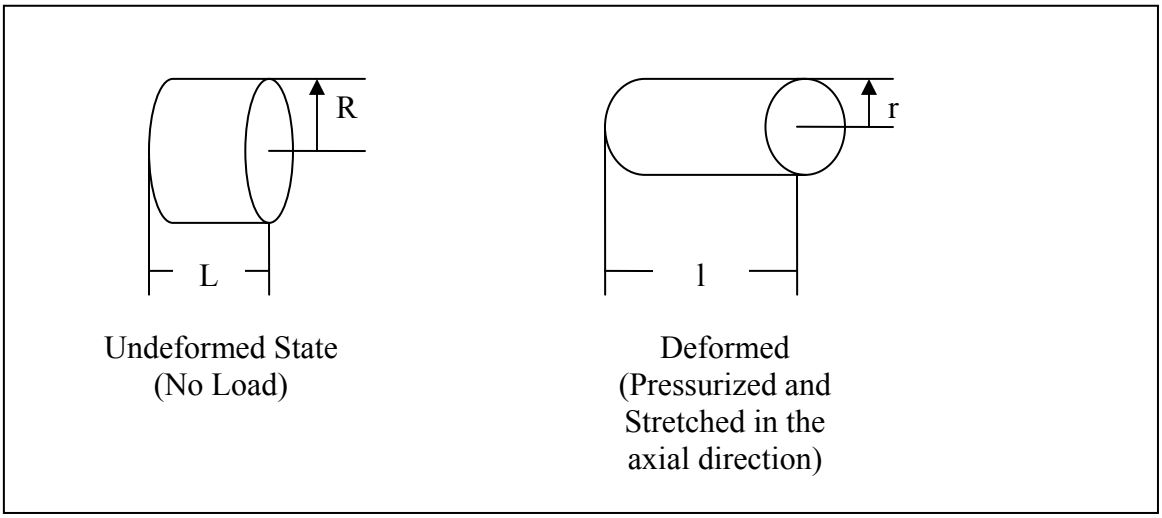

APPENDIX B: ARTERY TABLES

Table 5: Artery E (n=5)

E1	E2	E3	E4	E5
TT	TT	TT	TT	TT

Table 6: Artery F (n=3)

F1	F2	F3
TT	TT	TT

Table 7: Artery G (n=3)

G1	G2	G3
TT	TT	TT

Table 8: Artery L (n=8)

L1	L2	L3	L4	L5	L6	L7	L8
TT	CT (96%)	TT	CT (99%)	TT	CT (85%)	TT	CT (67%)

Table 9: Artery M (n=2)

M1	M2
TT	CT (40%)

Table 10: Artery O (n=6)

O1	O2	O3	O4	O5	O6
TT	CT (50%)	TT	CT (75%)	TT	CT (90%)

Table 11: Artery P (n=5)

P1	P2	P3	P4	P5
TT	TT	CT (80%)	TT	CT (50%)

Table 12: Artery R (n=5)

R1	R2	R3	R4	R5
TT	CT (66%)	TT	CT (90 %)	TT

Table 13: Artery T (n=5)

T1	T2	T4	T5
TT	CT (40%)	TT	CT (50%)

Table 14: Artery U (n=6)

U1	U2	U3	U4	U5	U6
TT	CT (60%)	TT	CT (40%)	TT	CT (50%)

Table 15: Artery V (n=4)

V1	V2	V3	V4
TT	CT (40%)	TT	CT (40%)

Table 16: Artery W (n=2)

W1	W2
TT	CT (28%)

Table 17: Artery Y (n=2)

T1	T2
TT	CT (80%)

Table 18: Artery Z (n=2)

T1	T2
TT	CT (23%)

APPENDIX C: DATA TABLE

Table 19: Data Table

Specimen	E1	E2	E3	E4	E5	F1
Test Percentage	1.00	1.00	1.00	1.00	1.00	1.00
ID (mm)	3.28	3.09	3.36	3.08	2.64	2.09
OD (mm)	5.52	4.42	5.03	4.75	4.20	4.76
Width, b (mm)	6.07	5.53	6.16	5.53	5.34	5.72
Thickness, t	2.23	1.33	1.67	1.68	1.55	2.67
Area, a	13.82	11.80	13.18	12.30	10.74	10.76
Initial Circumference, c	0.33	0.34	0.47	0.27	0.44	0.31
Final Position (in)	8.46	8.66	11.86	6.78	11.18	7.82
Final Position (mm)	15.79	16.20	22.60	12.44	21.23	14.52
Final Circumference (mm)	3.30	2.18	2.40	2.46	2.65	5.68
Final Force (lb.) (Input)	14.66	9.67	10.67	10.92	11.80	25.27
Final Force (N)	1.14	1.37	1.71	1.01	1.98	1.35
Stretch Ratio	0.62	0.90	0.89	0.60	1.40	1.12
Stress (MPa)	1.00	1.00	1.00	1.00	1.00	1.00
Pressure (mmHg)	1.08	1.31	1.03	1.18	1.42	1.65
N (Number of Cycles)	2353	2398	2652	1914	4783	6526

Specimen	F2	F3	G1	G2	G3
Test Percentage	1.00	1.00	1.00	1.00	1.00
ID (mm)	2.36	2.41	3.41	3.29	3.05
OD (mm)	3.62	3.69	4.93	4.94	5.01
Width, b (mm)	4.98	5.43	5.53	5.27	5.43
Thickness, t	1.25	1.28	1.52	1.65	1.96
Area, a	9.39	9.59	13.10	12.92	12.67
Initial Circumference, c	0.30	0.26	0.38	0.43	0.35
Final Position (in)	7.54	6.63	9.70	10.85	8.86
Final Position (mm)	13.96	12.13	18.28	20.57	16.60
Final Circumference (mm)	3.36	4.67	1.78	2.84	2.14
Final Force (lb.) (Input)	14.94	20.77	7.90	12.63	9.50
Final Force (N)	1.49	1.27	1.40	1.59	1.31
Stretch Ratio	1.78	1.89	0.66	1.16	0.58
Stress (MPa)	1.00	1.00	1.00	1.00	1.00
Pressure (mmHg)	2.39	2.98	0.94	1.45	0.89
N (Number of Cycles)	5592	5953	1795	3478	2131

Table 19 (Cont.)

Specimen	L1	L2	L3	L4	L5	L6
Test Percentage	1.00	0.80	1.00	0.90	1.00	0.85
ID (mm)	3.44	3.03	3.37	2.56	2.85	3.10
OD (mm)	5.46	5.26	5.21	4.44	5.15	5.08
Width, b (mm)	5.10	5.55	5.02	5.10	5.96	5.59
Thickness, t	2.03	2.22	1.84	1.87	2.30	1.98
Area, a	5.17	6.17	4.61	4.77	6.85	5.55
Initial Circumference, c	13.98	13.02	13.47	11.00	12.58	12.84
Final Position (in)	0.35	0.30	0.32	0.34	0.40	0.53
Final Position (mm)	8.86	7.65	8.13	8.74	10.24	13.56
Final Circumference (mm)	25.96	23.52	24.49	25.71	28.70	35.36
Final Force (lb.) (Input)	1.66	1.33	2.26	2.03	2.11	1.79
Final Force (N)	7.40	5.92	10.05	9.05	9.37	7.96
Stretch Ratio	1.86	1.81	1.82	2.34	2.28	2.75
Stress (MPa)	0.66	0.43	0.99	1.11	0.78	0.99
Pressure (mmHg)	2271	1744	3181	4447	3362	3592
N (Number of Cycles)	1	3	1	19	1	107

Specimen	L7	L8	M3	M4	O1	O2
Test Percentage	1.00	0.67	1.00	0.40	1.00	0.50
ID (mm)	2.91	3.45	2.80	2.62	3.55	3.55
OD (mm)	4.80	4.80	4.63	5.03	5.52	5.52
Width, b (mm)	5.61	6.02	4.98	5.57	5.03	5.03
Thickness, t	1.89	1.35	1.83	2.41	1.97	1.97
Area, a	5.30	4.07	4.55	6.71	4.97	4.97
Initial Circumference, c	12.11	12.97	11.68	12.02	16.58	16.58
Final Position (in)	0.51	0.54	0.36	0.30	0.44	0.52
Final Position (mm)	12.95	13.59	9.09	7.49	11.28	13.11
Final Circumference (mm)	34.14	35.41	26.42	23.22	30.79	34.44
Final Force (lb.) (Input)	2.78	1.87	4.06	1.62	2.16	1.08
Final Force (N)	12.38	8.32	18.06	7.23	9.59	4.79
Stretch Ratio	2.82	2.73	2.26	1.93	1.86	2.08
Stress (MPa)	1.65	1.40	2.25	0.52	0.90	0.50
Pressure (mmHg)	6053	3425	8281	2457	2927	1637
N (Number of Cycles)	1	389	1	4490	1	8667

Table 19 (Cont.)

Specimen	O3	O4	O5	O6	P1	P2
Test Percentage	1.00	0.75	1.00	0.90	1.00	1.00
ID (mm)	3.05	3.16	2.95	3.20	2.67	3.13
OD (mm)	5.11	5.12	4.67	5.10	5.20	5.09
Width, b (mm)	5.14	5.56	5.62	5.54	4.78	4.48
Thickness, t	2.05	1.96	1.72	1.90	2.54	1.96
Area, a	5.27	5.44	4.82	5.25	6.07	4.39
Initial Circumference, c	16.09	16.77	16.16	16.71	12.36	12.90
Final Position (in)	0.32	0.32	0.51	0.41	0.51	0.35
Final Position (mm)	8.10	8.08	13.03	10.31	13.03	8.86
Final Circumference (mm)	24.44	24.39	34.29	28.86	34.29	25.96
Final Force (lb.) (Input)	2.18	1.64	3.02	2.72	5.02	2.47
Final Force (N)	9.71	7.28	13.43	12.09	22.33	10.99
Stretch Ratio	1.52	1.45	2.12	1.73	2.77	2.01
Stress (MPa)	0.70	0.49	1.48	0.99	2.55	1.26
Pressure (mmHg)	2638	1725	4988	3406	12341	4503
N (Number of Cycles)	1	1157	1	37	1	1

Specimen	P3	P4	P5	R1	R2	R3
Test Percentage	0.80	1.00	0.50	1.00	0.67	1.00
ID (mm)	3.54	3.02	3.16	3.87	3.80	3.13
OD (mm)	5.16	5.37	5.52	5.10	4.53	4.87
Width, b (mm)	4.47	4.99	5.05	5.00	5.63	5.20
Thickness, t	1.62	2.35	2.36	1.23	0.73	1.74
Area, a	3.61	5.86	5.95	3.08	2.05	4.52
Initial Circumference, c	13.66	13.18	13.63	14.09	13.08	12.57
Final Position (in)	0.56	0.43	0.32	0.49	0.52	0.48
Final Position (mm)	14.15	11.02	8.22	12.32	13.13	12.14
Final Circumference (mm)	36.53	30.28	24.66	32.87	34.49	32.50
Final Force (lb.) (Input)	1.98	2.71	1.36	1.67	1.51	2.25
Final Force (N)	8.79	12.05	6.03	7.43	6.71	10.01
Stretch Ratio	2.67	2.30	1.81	2.33	2.64	2.59
Stress (MPa)	1.63	1.18	0.46	1.41	2.15	1.43
Pressure (mmHg)	4534	4954	1868	2898	2827	4667
N (Number of Cycles)	1098	1	8025	1	6640	1

Table 19 (Cont.)

Specimen	R4	R5	T1	T2	T4	T5
Test Percentage	0.90	1.00	1.00	0.40	1.00	0.50
ID (mm)	3.50	3.40	2.41	2.51	2.38	2.63
OD (mm)	4.20	5.13	3.97	4.00	3.61	3.60
Width, b (mm)	5.73	4.53	3.79	3.37	3.21	3.56
Thickness, t	0.70	1.73	1.56	1.50	1.23	0.97
Area, a	2.01	3.92	2.95	2.52	1.98	1.72
Initial Circumference, c	12.10	13.40	10.03	10.23	9.42	9.78
Final Position (in)	0.54	0.32	0.45	0.56	0.36	0.87
Final Position (mm)	13.64	8.00	11.46	14.20	9.04	22.14
Final Circumference (mm)	35.51	24.23	31.14	36.63	26.32	52.51
Final Force (lb.) (Input)	2.03	1.46	0.90	0.36	0.67	0.34
Final Force (N)	9.01	6.49	4.00	1.60	2.98	1.49
Stretch Ratio	2.94	1.81	3.11	3.58	2.79	5.37
Stress (MPa)	3.30	0.75	1.05	0.57	1.05	1.16
Pressure (mmHg)	4496	2280	3851	1961	3241	2707
N (Number of Cycles)	13	1		3371	1	10526

Specimen	U1	U2	U3	U4	U5	U6
Test Percentage	1.00	0.60	1.00	0.40	1.00	0.50
ID (mm)	2.90	2.75	2.53	2.59	2.56	2.58
OD (mm)	4.24	4.31	4.58	4.39	3.92	4.11
Width, b (mm)	3.22	3.51	3.32	3.01	3.41	3.23
Thickness, t	1.34	1.56	2.05	1.80	1.36	1.53
Area, a	2.16	2.74	3.41	2.72	2.32	2.48
Initial Circumference, c	11.71	12.28	12.41	11.63	11.51	11.53
Final Position (in)	0.51	0.42	0.55	0.62	0.36	0.39
Final Position (mm)	12.95	10.67	13.97	15.75	9.14	9.78
Final Circumference (mm)	34.14	29.57	36.17	39.73	26.52	27.79
Final Force (lb.) (Input)	0.53	0.32	0.61	0.24	0.52	0.26
Final Force (N)	2.36	1.41	2.71	1.09	2.31	1.16
Stretch Ratio	2.91	2.41	2.91	3.42	2.30	2.41
Stress (MPa)	0.80	0.31	0.58	0.34	0.57	0.28
Pressure (mmHg)	2245	1031	2511	1323	1808	968
N (Number of Cycles)	1	3221	1	2195	1	20056

Table 19 (Cont.)

Specimen	V1	V2	V3	V4	W1	W2
Test Percentage	1.00	0.40	1.00	0.40	1.00	0.28
ID (mm)	2.40	3.36	2.08	1.73	2.77	3.19
OD (mm)	3.93	5.55	3.78	4.22	4.72	5.21
Width, b (mm)	3.28	3.37	6.49	4.26	3.12	3.27
Thickness, t	1.53	2.20	1.70	2.50	1.94	2.02
Area, a	2.51	3.71	5.53	5.32	3.03	3.30
Initial Circumference, c	9.94	14.00	9.20	9.34	11.77	13.18
Final Position (in)	0.38	0.46	0.33	0.38	0.51	0.73
Final Position (mm)	9.53	11.63	8.38	9.55	12.95	18.44
Final Circumference (mm)	27.28	31.50	24.99	27.33	34.14	45.11
Final Force (lb.) (Input)	2.22	0.89	2.02	0.81	0.87	0.24
Final Force (N)	9.87	3.95	8.98	3.59	3.87	1.08
Stretch Ratio	2.74	2.25	2.72	2.93	2.90	3.42
Stress (MPa)	2.70	0.60	1.10	0.49	0.93	0.28
Pressure (mmHg)	9775	2218	4817	3114	3604	1013
N (Number of Cycles)	1	620	1	3597	1	65280

Specimen	Y1	Y2	Z1	Z2
Test Percentage	1.00	0.80	1.00	0.23
ID (mm)	3.41	3.22	2.87	2.56
OD (mm)	4.54	4.69	4.14	4.02
Width, b (mm)	3.50	3.62	5.56	5.80
Thickness, t	1.13	1.47	1.27	1.46
Area, a	1.98	2.67	3.52	4.22
Initial Circumference, c	12.49	12.42	11.02	10.33
Final Position (in)	0.19	0.35	0.42	0.62
Final Position (mm)	4.72	8.95	10.64	15.75
Final Circumference (mm)	17.68	26.13	29.52	39.73
Final Force (lb.) (Input)	0.69	0.55	0.81	0.19
Final Force (N)	3.07	2.46	3.60	0.83
Stretch Ratio	1.42	2.10	2.68	3.85
Stress (MPa)	0.55	0.48	0.69	0.19
Pressure (mmHg)	1170	1354	1857	627
N (Number of Cycles)	1	83	1	45791

REFERENCES

1. Suresh, S., *Fatigue of Materials*. Second ed. 1998: Cambridge University Press.

2. Dvorak, G.J.a.J., W.S., *Fatigue of Metal Matrix Composites.* International Journal of Fracture, 1980. **16**(6): p. 585-607.

3. Papageorgiou, G.L., and Jones, N.B., *Physical Modelling of the Arterial Wall. Part 1: Testing of Tubes of Various Materials.* Journal of Biomedical Engineering, 1986. **9**: p. 153-156.

4. McCord, B., *Fatigue of Atherosclerotic Plaque*, in *Mechanical Engineering*. 1993, Georgia Institute of Technology: Atlanta, GA. p. 154.

5. Ku, D.N., and Greene, P.R., *Scleral Creep In Vitro Resulting from Cyclic Pressure Pulses: Applications to Myopia.* American Journal of Optometry and Physiological Optics, 1981. **58**(7): p. 528-535.

6. Fung, Y.C., *Biomechanics - Mechanical Properties of Living Tissues*. 1993: Springer-Verlag.

7. Weizsacker, H.W., and Pinto, J.G., *Isotropy and Anisotropy of the Arterial Wall.* Journal of Biomechanics, 1988. **21**(6): p. 477-487.

8. Born, G.V.R., and Richardson, P.D., *Mechanical Properties of Human Athersclerotic Lesions*, in *Pathobiology of the Human Atherosclerotic Plaque*, N. Glagov, Schaffer, Editor. 1990.

9. Humphrey, J.D., *Mechanics of the Artorial Wall: Review and Directions.* Critical Reviews in Biomedical Engineering, 1995. **23**(1&2): p. 1-141.

10. Tanaka, T.T., and Fung., Y.C., *Elastic and Inelastic Properties of the Canine Aorta and Their Variation Along th Aortic Tree.* Journal of Biomechanics, 1974. **7**: p. 357-370.

11. Purslow, P.P., *Positional Variations in Fracture Toughness, Stiffness and Strength of Descending Thoracic Pig Aorta.* Journal of Biomechnics, 1983. **16**(11): p. 947-953.

12. Mohan, D., and .Melvin, J.W., *Failure Properties of Passive Human Aortic Tissue I-Uniaxial Tension Tests.* Journal of Biomechanics, 1982. **15**(11): p. 887-902.

13. Rachev, A., *Theoretical Study of the Effect of Stress-Dependent Remodeling on Arterial Geometry Under Hypertensive Conditions.* Journal of Biomechanics, 1997. **30**(8): p. 819-827.

14. Cox, R.H., *Passive Mechanics and connective tissue composition of canine arteries.* American Journal of Phyiology, 1978. **234**(5): p. H533-H541.

15. Constantinides, P., *Plaque Fissure in Human Coronary Thrombosis.* Journal of Atherosclerotic Research, 1966. **6**: p. 1.

16. Cheng, G.C., Loree, H.M., Kamm, R.D., Fishbein, M.C., and Lee, R.T., *Disruption of Circumferential Stress in Ruptured and Stable Atherosclerotic Lesions.* Circulation, 1993. **87**: p. 1179-1187.

17. Falk, E., Shah, P.K. and Fuster, V., *Coronary Plaque Disruption.* Circulation, 1995. **92**(3): p. 657-671.

18. Richardson, P.D., Davies, M.J., and Born, G.V.R., *Influence of Plaque Cnfiguration and Stress Distribution on Fissuring of Coronary Atherosclerotic Plaques.* The Lancet, 1981. **2**: p. 941-944.

19. Ambrose, J.A., Tannenbaum, M.A., Alexopoulos, D., Hjemdahl-Monsen, C.E., Leavy, J., Weiss, M., Borrico, S., Gorlin, R., and Fuster, V., *Angiographic Progression of Coronary Artery Disease and the Development of Myocardial Infarction.* J Am Coll Cardiol, 1988. **12**: p. 56-62.

20. Chandler, A., *Mechanisms and frequency of thrombosis in the coronary circulation.* Thromb. Res., 1974. **4**: p. 3-22.

21. Lendon, C.L., Davies, M.J., Born, G.V.R., and Richardson, P.D., *Atherosclerotic Plaque Caps are locally weakened when macrophages density is increased.* Atherosclerosis, 1991. **87**: p. 87-90.

22. Gertz, S.D., and Roberts, W.C., *Hemodynamic Shear Force in Rupture of Coronary Arterial Atherosclerotic Plaques.* The American Journal of Cardiology, 1990. **66**: p. 1368-1372.

23. Loree, H.M., Kamm, R.D., Atkinson, C.M. and Lee, R.T., *Turbulent Fluctuations on Surface of Model Vascular Stenoses.* American Journal of Physiology, 1991. **261**(30): p. H644-H650.

24. Richardson, P.D., Davies, M.J., and Born, G.V.R., *Influence of Plaque Cnfiguration and Stress Distribution on Fissuring of Coronary Atherosclerotic Plaques.* The Lancet, 1989. **2**: p. 941-944.

25. Lee, R.T., Grodzinsky, A.J., Frank, E.H., Kamm, R.D., and Schoen, F.J., *Structure-Dependent Dynamic Mechanical Behavior of Fibrous Caps From Human Atherosclerotic Plaques.* Circulation, 1991. **83**: p. 1764-1770.

26. Vito, R.P., Whang, M.C., Giddnes, D.P., Zarins, C.K. and Glagov, S., *Stress Analysis of the Diseased Arterial Cross-Section.* p. 273-276.

27. Loree, H.M., Kamm, R.D., Stringfellow, R.G. and Lee, R.T., *Effects of Fibrous Cap Thickness on Circumferential Stress in Model Atherosclerotic Vessels.* Circulation Research, 1992. **71**: p. 850-858.

28. Shah, P.K., *Plaque Disruption and Coronary Thrombosis: New Insight into Pathogenesis and Prevention.* Clin. Cardiol., 1997. **20 (Suppl. II)**(II): p. II-38-II-44.

29. Carmines, D.V., McElhaney, J.H., and Stack, R., *A Piece-Wise Non-Linear Elastic Stress Expression of Human and Pig Coronary Arteries Tested In Vitro.* Journal of Biomechanics, 1991. **24**(10): p. 899-906.

30. van Andel, C.J., Pistecky, P.V., and Borst, C., *Mechanical Properties of Porcine and Human Arteries: Implications for Coronary Anastomotic Connectors.* Annals of Thoracis Surgery, 2003. **76**: p. 58-65.

31. Holzapfel, G.A., Sommer, G., and Regitnig, P., *Anisotropic Mechanical Properties of Tissue Components in Human Atherosclerotic Plaques.* Jounarl of Biomechanical Engineering, 2004. **126**: p. 657-665.

32. Sokolis, D.P., Boudoulas, H., and Karayannacos, P.E., *Assessment of the aortic stress-strain relation in uniaxial tension.* Journal of Biomechanics, 2002. **35**: p. 1213-1223.

33. Mohan, D., and Melvin, J.W., *Failure Properties of Passive Human Aortic Tissue II-Biaxial Tension Tests.* Journal of Biomechanics, 1982. **16**(1): p. 31-44.

34. Quapp, K.M., Weiss, J.A., *Material Characterization of Human Medial Collateral Ligament.* Journal of Biomechanical Engineering, 1998. **120**: p. 757-763.

35. Weiss, J.A., Gardiner, J.C., Bonifasi-Lista, Carlos, *Ligament material behavior is nonlinear, viscoelastic and rate-independent under shear loading.* Journal of Biomechanics, 2002. **35**: p. 943-950.

36. Johnson, G.A., Tramaglini, Dawn M., Levine, Rebecca E., Ohno, Kazunori, Choi, Nam-Yong, Woo, Savio L-Y, *Tensile and Viscoelastic Properties of Human Patellar Tendon.* Journal of Orthopaedic Research, 1993. **12**: p. 796-803.

37. Itoi, E., Berglund, L.J., Grabowski, J.J., Schultz, F.M., Growney, E.S., Morrey, B.F., and Kai-Nan, A., *Tensile Properties of Supraspinatus Tendon.* Journal of Orthopaedic Research, 1995. **13**: p. 578-584.

38. Haut, R.C., Garg, B.D., Metke, M., Jose, M. and Kaye, M.P., *Mechanical Properties of the Canine Aorta Following Hypercholesterolemia.* Journal of Biomechanical Engineering, 1980. **102**: p. 98-102.

39. Lally, C., Reid, A.J., and Pendergast, P.J., *Elastic Behavior of Porcine Artery Tissue under Uniaxial and Equibiaxial Tension.* Annals of Biomedical Engineering, 2004. **32**(10): p. 1355-1364.

40. Broom, N.D., *The Stress/Strain and Fatigue Behaviour of Glutaraldehyde Preserved Heart-Valve Tissue.* Journal of Biomechanics, 1977. **10**: p. 707-724.

41. Wells, S.M., and Sacks, M.S., *Effects of fixation pressure on the biaxial mechanical behavior of porcine bioprosthetic heart valves with long-term cyclic loading.* Biomaterials, 2001. **23**: p. 2389-2399.

42. Yokobori, A.T., Maeyama, T., Ohkum, T., Yokobori, T. et al., *Bio-Medico-Mechanical Behavior of Natural Artery Blood Vessel Under Constant and Variable Internal Pulsatile Pressure Flow Test In Vitro.* Journal of Biomechanical Engineering, 1986. **108**: p. 295-300.

43. Beer, F.P., and Johnston, E.R., *Mechanics of Materials*. 2nd ed. 1992: McGraw-Hill, Inc.

44. Mendenhall, W., *Introduction to Probability and Statistics*. 3rd ed. 1971: Duxbury.

45. Okamoto, R.J., Wagenseil, J.E., DeLong, W.R., Peterson, S.J., Kouchoukos, N.T., and Sundt, T.M., *Mechanical Properties of Dilated Human Ascending Aorta.* Annals of Biomedical Engineering, 2002. **30**: p. 624-635.

46. Lendon, C.L., Briggs, A.D., Born, G.V.R., Burleigh, M.C. and Davies, M.J., *Mechancial Testing of connective tissue i the search for determinants of atherosclerotic plaque cap rupture.* Biochemical Sociey Transactions, 1988. **627th Meeting**: p. 1032-1033.

47. Chin Quee, S.L.H., *Design Verification for Tissue Engineered Vascular Grafts*, in *Mechanical Engineering*. 2001, Georgia Institute of Tehcnology: Atlanta, GA.

48. Altus, E., *Nonlinear differential equation for fatigue damage evolution, using a micromechanical model.* Mechanics of Materials, 2002. **34**: p. 257-266.

50. Dowling, N.E. *Mechanical Behavior of Materials*, 2nd ed. 1999: Prentice-Hall.